UNCLASSIFIED

AD NUMBER: AD0469130

LIMITATION CHANGES

TO:

Approved for public release; distribution is unlimited.

FROM:

Distribution authorized to US Government Agencies and their Contractors; Administrative/Operational Use; 1 Jun 1965. Other requests shall be referred to Aeronautical Systems Division, Wright-Patterson AFB, OH 45433.

AUTHORITY

ASD ltr dtd 21 Jan 1970

THIS PAGE IS UNCLASSIFIED

CATALOGED BY DDC
AS AD No. 469130

ARL 65-118
JUNE 1965

Aerospace Research Laboratories

A STUDY ON THE PERFORMANCE POTENTIAL OF CONVENTIONAL AND SHEAR FORCE PUMPS

O. E. BALJE
ENGINEERING CONSULTANT
SHERMAN OAKS, CALIFORNIA

DDC
RELEASED
SEP 9 1965
DDC-IRA E

OFFICE OF AEROSPACE RESEARCH
United States Air Force

SECURITY MARKING

The classified or limited status of this report applies to each page, unless otherwise marked.
Separate page printouts MUST be marked accordingly.

THIS DOCUMENT CONTAINS INFORMATION AFFECTING THE NATIONAL DEFENSE OF THE UNITED STATES WITHIN THE MEANING OF THE ESPIONAGE LAWS, TITLE 18, U.S.C., SECTIONS 793 AND 794. THE TRANSMISSION OR THE REVELATION OF ITS CONTENTS IN ANY MANNER TO AN UNAUTHORIZED PERSON IS PROHIBITED BY LAW.

NOTICE: When government or other drawings, specifications or other data are used for any purpose other than in connection with a definitely related government procurement operation, the U. S. Government thereby incurs no responsibility, nor any obligation whatsoever; and the fact that the Government may have formulated, furnished, or in any way supplied the said drawings, specifications, or other data is not to be regarded by implication or otherwise as in any manner licensing the holder or any other person or corporation, or conveying any rights or permission to manufacture, use or sell any patented invention that may in any way be related thereto.

NOTICES

When Government drawings, specifications, or other data are used for any purpose other than in connection with a definitely related Government procurement operation, the United States Government thereby incurs no responsibility nor any obligation whatsoever; and the fact that the Government may have formulated, furnished, or in any way supplied the said drawings, specifications, or other data, is not to be regarded by implication or otherwise as in any manner licensing the holder or any other person or corporation, or conveying any rights or permission to manufacture, use, or sell any patented invention that may in any way be related thereto.

- - - - - - - - - -

Qualified requesters may obtain copies of this report from the Defense Documentation Center, (DDC), Cameron Station, Alexandria, Virginia.

(Reproduction in whole or in part is permitted for any purpose of the U.S. Govt.)

- - - - - - - - - -

DDC release to OTS not authorized

- - - - - - - - - -

Copies of ARL Technical Documentary Reports should not be returned to Aerospace Research Laboratories unless return is required by security considerations, contractual obligations or notices on a specified document.

300 - July 1965 - 448-50-1076

ARL 65-118

A STUDY ON THE PERFORMANCE POTENTIAL OF CONVENTIONAL AND SHEAR FORCE PUMPS

O. E. BALJE

ENGINEERING CONSULTANT
SHERMAN OAKS, CALIFORNIA

Contract AF 33(615)-1915

AERONAUTICAL RESEARCH LABORATORIES
OFFICE OF AEROSPACE RESEARCH
UNITED STATES AIR FORCE
WRIGHT-PATTERSON AIR FORCE BASE, OHIO

Foreword

This report was prepared under USAF Contract No. AF33(615)-1915, with Mr. S. Hasinger, Task Scientist, acting as Project Engineer.

Abstract

The design point performance of shear force pumps is compared with that of conventional pumps in terms of the similarity parameters specific speed, specific diameter and suction specific speed. Using arguments of the cascade theory, the maximum suction specific speed potential of conventional pumps is calculated for conventional as well as sophisticated blade design concepts. Comparing these data with experimental and theoretical data of shear force pumps, it was demonstrated that shear force pumps can obtain about 10 to 20 times higher suction specific speeds than conventional pumps in the medium specific speed regime, but that the efficiency potential of shear force pumps is lower than that of conventional pumps. The high suction specific speed potential of the shear force pump can be used advantageously in the design of compact lightweight space powerplants.

Summary

The advances in the potential flow theory allow to precalculate the pressure distribution around the airfoil in cascades and thus to establish the suction specific speed potential of conventional pumps. It was found that with conventional design methods, high suction specific speeds are obtained with high specific speed axial pumps, reaching peak values of 1000, but that the suction specific speed potential decreases to about 400 in the medium and low specific speed regimes. With refined blade design concepts, suction specific speed of 1000 can be obtained over the whole specific speed regime of conventional pumps. It was assumed in these calculations that tip clearance cavitation can be avoided with proper gap

control or by providing a shroud. The suction specific speed potential of pitot pumps appears to be higher than that of conventional pumps, reaching peak values of about 3000.

By investigating the efficiency potential of conventional pumps it is found that pumps designed for maximum suction specific speed tend to require a cascade geometry which will compromise the efficiency to some degree. An exception is the mixed flow pump, where the cascade geometry desired for obtaining high efficiencies will also be suitable for obtaining high suction specific speeds.

The analysis of the shear force pump reveals that this pump type will reach peak efficiencies in the medium to low specific speed regimes, but that these efficiency values are smaller than the ones obtained with conventional pumps in this specific speed range. The suction specific speed potential of shear force pumps, however, is considerably higher than that of conventional pumps, reaching values as high as 20,000. Thus, the most feasible application of shear force pumps is for installations where the efficiency can be compromised in favor of high suction specific speeds. Typical applications are condensate pumps in space power plants of the Rankine cycle type where the high suction specific speed allows a reduction in sub-cooler area and weight, thus decreasing the specific weight of space powerplants.

The presently available test evidence on shear force pumps covers only the rotor performance. Since the efficiency of shear force pumps depends in large measure on the diffuser efficiency, efficient diffuser geometries have to be developed before the shear force pump can be applied for the proposed application.

A STUDY ON THE PERFORMANCE POTENTIAL OF CONVENTIONAL AND SHEAR FORCE PUMPS

Table of Contents

LIST OF FIGURES

Introduction

Recent investigations on shear force pumps (reference 1, 2) indicate that this pump type has a particularly low cavitation sensitivity and might be particularly suitable for low specific speed operation, i.e., in operating regimes where conventional pumps have a low efficiency potential. It is therefore of interest to compare the cavitation performance as well as efficiency potential of shear force pumps with that of conventional pumps. Fluid dynamic similarity considerations offer a realistic basis for this comparison.

Definition of Parameters

In order to insure general validity of the comparison, significant parameters must be defined which represent the fluid dynamic aspect of the different pump types adequately. It has been demonstrated (reference 3) that the similarity parameters (1) specific speed N_s, (2) specific diameter D_s, (3) suction specific speed S^* and (4) Reynolds Number R_e^* describe the design point characteristic of conventional pumps completely. They have the same validity for shear force pumps, although the pumping mechanism in the rotor of shear force pumps is different from that of conventional pump rotors. It is, nevertheless, important to realize that the off-design performance of conventional pumps differs significantly from that of shear force pumps due to the difference in the rotor flow mechanism. Hence, the comparison has to distinguish between two phases; (1) design point performance and (2) off-design performance of the different pump types.

For the design point performance comparison, the similarity parameters N_s, D_s, S^* and R_e^* will be used, whose derivation is presented in reference 3 and may be summarized as follows:

The specific speed N_s is a term which interrelates the rotative speed N with the pump design flow V_1 and design pressure head H_{ad}, and is defined by the relation

$$N_s = \frac{N\sqrt{V_1}}{H_{ad}^{3/4}} \tag{1}$$

when N is quoted in RPM, V_1 in ft^3/sec (volume flow at pump inlet) and H_{ad} in ft.

The specific diameter interrelates the rotor diameter D (in ft.) with the pump design flow and design pressure head,

$$D_s = \frac{D\,H_{ad}^{1/4}}{\sqrt{V_1}} \tag{2}$$

The Reynolds Number is used to express the influence of the inlet condition and pump size and, for convenience, is defined by

$$Re^* = \frac{u_2 D}{\nu_1} \tag{3}$$

when u_2 denotes the rotor tip speed and ν_1 the kinematic viscosity of the fluid at pump inlet.

The suction specific speed interrelates the rotative speed and pump design flow with the cavitation suppression head H_s (ft.) required to avoid incipient cavitation

$$S^* = \frac{N\sqrt{V_1}}{H_s^{3/4}} \tag{4}$$

It is to be noted that the term suction specific speed, as used in this report, defines the condition where incipient cavitation occurs, rather than the point where the performance starts to drop. This distinction is significant, since cavitation inception occurs earlier, i.e., at higher cavitation suppression heads than performance dropoff. Thus, in general, suction specific speed values quoted for incipient cavitation are lower than those associated with performance dropoff. It can usually be assumed that no cavitation damage occurs as long as the suction specific speed is higher than the suction specific speed for incipient cavitation. More specifically, the suction specific speed as used in this report indicates the operation condition where the lowest blade surface pressure is equal to the vapor pressure. Actually this suction specific speed is the only cavitation parameter which can be rigorously defined on the basis of fluid dynamic considerations. Whether or not cavitation actually does occur at this operating condition depends on other criteria, particularly thermodynamic parameters which cannot be derived from fluid dynamic similarity considerations. Thus, additional thermodynamic parameters have to be used in order to indicate the chances of cavitation actually occurring. Since the comparison presented here is only concerned with fluid dynamic aspects, no comments will be offered on the comparison of the thermodynamic cavitation criteria (sometimes referred to as dissimilarity parameters) of conventional pumps and shear force pumps.

The significance of the quoted similarity parameters may be demonstrated by discussing Figure 1 which shows lines of constant (total to static) efficiencies for axial pumps as function of specific speed and specific diameter. It may be

recalled, as demonstrated in detail in reference 3, that geometrically similar pumps having the same specific speed and specific diameter exhibit the same velocity triangles, i.e., have similar flow vectors, and thus have the same efficiency as long as the loss coefficients, (i.e., the Reynolds Number) are the same. Thus, an interrelation between efficiency, specific speed, specific diameter, loss coefficient and pump geometry can be derived. By partial differentiation of this relation, the optimum geometry for given N_s and D_s values can be found (for fixed values of the Reynolds Number) so that eventually an interrelation for the maximum efficiency as function of N_s and D_s results. This information is plotted in Figure 1, meaning that every point on this diagram is a design point. In the course of this optimization, the optimum geometry for given N_s and D_s values also has been determined, which now can be represented as function of N_s and D_s in terms of lines of constant hub ratio (shown also in Figure 1), lines of constant rotor inlet angle, constant rotor exit angle, constant diffuser inlet angle, constant diffuser exit angle, constant blade heights to diameter ratios, constant pitch chord ratios, constant chord length to rotor diameter ratios, etc. Such a diagram then represents the maximum obtainable pump efficiency and the associated optimum geometry for a fixed values of the Reynolds Number. It is to be noted that the interrelation between cascade geometry and loss coefficient is necessarily a function of the state-of-the-art. Since this interrelation has to be used in order to arrive at Figure 1, the efficiency values quoted there are also an expression of the state-of-the-art.

The required cavitation suppression head H_s for avoiding incipient cavitation can be calculated by using potential flow arguments. On this basis, the pressure

distribution or velocity distribution along the blade surface can be calculated as function of cascade stagger angle, flow deflection (lift coefficient), pitch chord ratio and blade thickness. A typical surface velocity distribution is shown in Figure 2 by plotting the ratio of surface velocity W to average velocity W_∞ (see Figure 5 for definition) as function of the chord length x^*/C. This diagram indicates that the surface velocity at the suction side of the profile first increases with increasing chord lengths and then decreases, reaching a maximum value at about 30% of the chord length. This means that the blade surface pressure at the suction side reaches lower values than the static pressure at cascade inlet. In order to avoid cavitation inception, the vapor pressure of the fluid must not rise above the lowest blade surface pressure. Hence, the difference between the lowest suction side blade surface pressure and static inlet pressure is a significant criterion for calculating the cavitation suppression head and, consequently, the suction specific speed.

Evaluating these relations numerically, the suction specific speed can be calculated and presented by lines of constant S^* values, as shown in Figure 1 by dashed lines. These data indicate that S^* increases with increasing specific speeds, and that the regime of maximum suction specific speeds occurs at specific diameter values which are smaller than D_s values for maximum efficiencies.

It is apparent that the presentation of the design point performance in the form of an $N_s D_s$ diagram, as shown in Figure 1, allows to recognize the main pump criteria, such as efficiency and suction specific speed, as function of the similarity parameters N_s and D_s reflecting speed and rotor size, in a convenient

and technically rigorous form. The fact that such a diagram can be valid only for a limited range of Reynolds Numbers is usually not too severe a handicap, since pump Reynolds Numbers in most cases are comparatively high and therefore in a regime where pump performance is only very little affected by Reynolds Number effects. Thus, the $N_s D_s$ presentation will be used as a basic tool for the performance comparison.

Design Point Performance of Conventional Pumps

Efficiency Relations

In previous studies (references 3, 4 and 5) a series of $N_s D_s$ diagrams have been generated, which show the maximum obtainable pump efficiency for single stage piston pumps, pitot pumps, centrifugal pumps, axial pumps and drag pumps. The most pertinent data of these studies are presented in Figure 3, which might be described as follows: Axial pumps are most efficient at high specific speeds, particularly in regimes between N_s = 300 to 800. In the specific speed regime between 60 and 120, centrifugal pumps are most efficient, reaching values of 90% and better at specific speeds above 100. The optimum specific diameters for centrifugal pumps are higher than the corresponding values for axial pumps, indicating higher tip speeds and, consequently, higher pump heads. In the specific speed regime between 150 and 300, mixed flow pumps give best performance, reaching efficiency levels as high as centrifugal pumps and axial pumps.

A variety of pumps has to be considered in the low specific speed regime. Considering dynamic devices first, partial emission pumps and pitot pumps offer a fair efficiency potential; the partial emission pump covering the specific speed

regime from 10 to 25, and the pitot pump covering even lower specific speeds. In general, the efficiency potential of dynamic devices, as described sofar, tends to be restricted to comparatively low values in the low specific speed regime. Actually it is possible to plot a limit line for dynamic devices in the $N_s D_s$ diagram if it is considered that the maximum head coefficient obtainable in dynamic devices is unlikely to exceed a value of $\eta_{ad} = 1.3$. Remembering now that the head coefficient is interrelated with specific speed and specific diameter (equation (15)), a 45° line can be plotted in the $N_s D_s$ diagram, indicating the limit line for the performance of dynamic devices. This is shown by the heavy solid line in Figure 3.

Partial emission pumps are modified centrifugal pumps with a rotor design similar to that for centrifugal pumps, but a diffuser and collector scroll area modified in such a manner that the flow discharge from the impeller is allowed to leave the impeller only over a comparatively small section of the periphery. The flow is collected in a small segment and then guided through a single conical diffuser, as schematically shown in Figure 4. With this arrangement, the diffuser efficiencies are improved if compared with conventional full admission devices. Thus, this pump type gives higher efficiencies than conventional centrifugal pumps in the low specific speed regime.

It is of interest to remember at this point that high specific speed devices have skin friction losses as the major loss source, whereas low specific speed devices have wheel disc friction as a major source for the inefficiency. Hence, in order to obtain efficient low specific speed devices, wheel disc friction losses

have to be minimized. This is accomplished in pitot pumps, schematically shown in Figure 4, by having the rotor operate in a medium (ambient air) which has a lower density than the density of the pumped fluid. Since wheel disc friction losses are proportional to the density of the surrounding medium a considerable improvement in efficiency can be obtained when, for example, pumping water with these devices, since the density ratio between the surrounding air and the pump liquid is about 1/800. With this assumption, the performance presented in Figure 3 was calculated for pitot pumps. It is then also evident that lower efficiencies than quoted in Figure 3 will result for pitot pumps in cases where the density ratio is higher than 1/800.

Displacement devices usually are performing best at low and ultra low specific speeds. The results of detailed calculations of the performance of single plunger piston pumps (reference 4) are also shown in Figure 3, indicating high efficiencies in the ultra low specific speed regime. Since the working principles of displacement devices are considerably different from the working principle in dynamic machines, one would not expect that the performance characteristic of displacement devices can be represented by parameters originally derived from dynamic machinery. In analyzing, however, the loss relations for displacement devices (reference 3), it was found that the similarity parameters, specific speed and specific diameter, have the same validity for displacement machines as they have for dynamic devices.

In specific speed regimes between 1 and 30, vane type pumps and Roots pumps show best efficiencies, as indicated by lines of constant efficiency for these devices

in Figure 3. Additional lines in the $N_s D_s$ diagram indicate the optimum geometry required for obtaining the quoted efficiencies, namely, the stroke to bore ratio S^*/D for piston machines, the rotor length to diameter ratio L/D for Roots and vane pumps, the hub ratio λ for axial pumps, the rotor diameter ratio ϵ for centrifugal pumps and the ratio D/Δ for pitot pumps, Δ denoting the bore diameter of the pitot head. The efficiency values, shown in Figure 3, are calculated by assuming certain clearance values s between rotor and stator, as indicated by the quoted clearance ratios s/D.

The performance potential of drag pumps is also indicated in Figure 3, revealing a somewhat limited efficiency potential, namely, a maximum of about 50% occurring at specific speeds between 3 and 10. The drag pumps can be classified as a hybrid between displacement devices and dynamic devices, or they could be interpreted as a multi-stage dynamic device. It is therefore not too surprising that the maximum performance potential is obtained in the performance regime between displacement machines and dynamic devices. It is also interesting to note that displacement devices have a smaller specific diameter, i.e., require a smaller rotor size than dynamic devices, as it becomes evident by comparing the specific diameters of pitot pumps with that of vane type pumps.

The information supplied in Figure 3 may suffice to indicate the design performance potential of pumps as function of specific speed.

Suction Specific Speed Relations

In order to calculate the suction specific speed of dynamic devices, the surface velocity distribution along the blade contour, schematically shown in Figure 2, has to be evaluated numerically. Actually, it is conventional practice to define the cavitation suppression head as the difference between total inlet pressure and vapor pressure. Thus, the cavitation suppression head becomes

$$H_s = \frac{p_{1-t} - p_{vapor}}{\gamma} \tag{5}$$

Using now velocity heads instead of pressure heads, the required cavitation suppression head can be quoted in the form

$$H_s = \frac{c_1^2}{2g} + k_5 \frac{w_1^2}{2g} \tag{6}$$

when c_1 denotes the axial velocity at rotor inlet and w_1 the relative velocity in the rotor channel (Figure 5). The factor k_5 in equation (6) can then be calculated from the surface velocity distribution shown in Figure 2. A general interrelation between velocity distribution and cascade parameters for circular arc profiles is presented in reference 6, leading tc an interrelation between the surface velocity w and average channel velocity w_∞ as function of pitch chord ratio S/C, the cascade stagger angle β_∞, the lift coefficient C_L and the profile thickness ratio t/C. The average channel velocity w_∞ can be related to the relative inlet velocity w_1, yielding for the factor k_5 a relation of the form

$$k_5 = \left(k_6^2 - 1\right)\left(\frac{\sin\beta_1}{\sin\beta_\infty}\right)^2 \tag{7}$$

with

$$k_6 = \frac{w}{w_\infty} \tag{8}$$

Evaluating equation (8) numerically on the basis of reference 6 for circular arc camber lines, it results that k_6 reaches a maximum at about 30% of the chord length (Figure 2), and that for this chord position, k_6 increases linearly with increasing ratios of C_L x C/S for small stagger angles, as shown in Figure 6. This means that the minimum surface pressure occurs at about 30% chord length, so that at this chord position cavitation inception has to be expected, Since the parameter C_L x C/S is interconnected with the blade loading, representing flow deflection

$$C_L \frac{C}{S} = 2 \frac{\Delta W_u}{W_\infty} \tag{9}$$

i.e., cascade geometry, which already has been calculated for efficiency-optimized pump designs in Figure 1 and 3, it becomes evident that lines of constant k_6 values can be plotted in Figure 1, or even better, lines of constant suction specific speed.

Actually, the suction specific speed information can be presented in two different forms; (1) by lines of constant S^* values, dashed lines in Figure 1, and (2) by showing only the operating regime where maximum suction specific speeds occur, dotted line in Figure 1. In order to recognize important trends, the first method may be explored by applying equations (5) to (9) to the design criteria of axial pumps. Restricting these considerations to a blade thickness ratio of t/C = .01, it follows from Figure 6 that the velocity ration w/w_∞ can be represented by the relation

$$k_6 = 1.02 + .3 C_L \frac{C}{S} = 1.02 + \frac{.6 \Delta W_u}{W_\infty} \tag{10}$$

and the cavitation parameter k_5, after introducing equation (10) into equation (7) by the relation

$$K_5 = \left(\frac{\sin\beta_1}{\sin\beta_\infty}\right)^2 \left[\left(1.02 + \frac{.6\,\Delta w_u}{w_\infty}\right)^2 - 1\right] \tag{11}$$

The terms on the right hand side of equation (11) can now be expressed by the similarity parameters, as may be demonstrated by the following considerations: The head, generated by the pump is

$$H_{ad} = \frac{u_2\,\Delta w_u}{g}\,\eta_h \tag{12}$$

when η_h denotes the hydraulic efficiency and u_2 the peripheral wheel tip speed. Thus

$$\Delta w_u = \frac{H_{ad}\,g}{u_2\,\eta_h} = \frac{q_{ad}}{\eta_h}\,u_2 \tag{13}$$

with

$$q_{ad} = \frac{H_{ad}\,g}{u_2^2} \tag{14}$$

denoting a pump head coefficient which is interrelated with the similarity parameters by

$$q_{ad} = \frac{g\,60^2}{N_s^2\,D_s^2\,\pi^2} \tag{15}$$

The average flow velocity w_∞ can be expressed by the relation

$$w_\infty = u_2\sqrt{R^2 - q_{ad}\,\eta_h + \left(\frac{q_{ad}\,\eta_h}{2R}\right)^2 + \varphi^2} \tag{16}$$

when $R = r/r_a$ denotes the radius ratio; φ denotes a flow factor

$$\varphi = \frac{c_{m_1}}{u_2} \tag{17}$$

which is interrelated with N_s and D_s by

$$\varphi = \frac{240}{\pi^2 N_s D_s^3 (1-\lambda^2)} \tag{18}$$

$\lambda = d_h/D$ denoting the rotor hub ratio. The velocity triangles, shown in Figure 5, indicate that β_1 and β_∞ can be expressed by c_m, u and w_∞ i.e., by N_s and D_s (after considering equation (16) and (17)). Introducing these relations into equation (11) and subsequently into equations (6) and (4), a relation for the suction specific speed as function of specific speed, specific diameter hub ratio and hydraulic efficiency of the form

$$S^* = \frac{16.3\, N_s D_s^3 (1-\lambda^2)}{\left[1.04 + (1-\lambda^2)^2 \frac{24.6\, D_s^4}{\eta_h} \sqrt{1 - \frac{1.16\times10^4}{\eta_h N_s^2 D_s^2} + \frac{3.35\times10^7}{\eta_h^2 N_s^4 D_s^4} + \frac{576}{N_s^2 D_s^4 (1-\lambda^2)^2} + (1-\lambda^2)^2 \left(\frac{1.07\times10^4 D_s^2}{\eta_h^2 N_s^2} + \frac{N_s^2 D_s^4}{1.44\times10^4} \right)} - \frac{.8 D_s^4}{\eta_h} \right]^{3/4}} \tag{19}$$

results for axial pumps.

Using now efficiency values and hub ratios resulting from the previously calculated $N_s D_s$ diagram for axial pumps, Figure 1 (i.e., pump geometries optimized for maximum efficiency) equation (19) can be evaluated numerically, yielding lines of constant suction specific speed, as indicated by the dashed lines in Figure 1. It is interesting to note that the available experimental evidence supports the calculated S^* in the medium specific speed regime, as evidenced by the test points shown in Figure 1, obtained from references 7 and 8 by converting the operating conditions for incipient cavitation into N_s and D_s values.

It is important to note that the lowest suction specific speed, i.e., maximum required cavitation suppression head, occurs at the rotor tip, due to the comparatively large value of the relative velocity w_1 at this point. A

typical example for the required cavitation suppression head for the smaller radii is shown in Figure 7, which quotes the suction specific speed for different radii of a given design (straight axial inlet flow without preswirl assumed) indicating considerably higher suction specific speed in the hub regime.

It should also be noted that the suction specific speed values shown in Figure 1 neglect the influence of the gap between blade tip and stator. Actually, in unshrouded designs, tip clearance cavitation usually sets in before blade surface cavitation occurs. The tip clearance flow is generated by the pressure difference between suction and pressure side of the blade, causing a low pressure regime in the gap. Also the eddy shed from the tip clearance flow has frequently been observed to have low pressure regimes inside of the vortex street, which again can cause cavitation. Recent investigations (reference 7) have shown that gap cavitation can be minimized by proper selection of the gap geometry.

By providing a shroud around the tips, gap cavitation can be eliminated. Hence, blade surface cavitation can be expected to occur first, so that for this design concept the calculated suction specific speed values are rigorous. The pump efficiencies shown in Figures 1 and 3 are, however, calculated for designs without tip shroud. Significantly lower pump efficiencies can result when a tip shroud is assumed, since high shroud windage losses can occur. The magnitude of these losses depends on the axial length of the shroud. Actually, another optimization parameter, axial rotor length to rotor diameter, would have to be determined for

shrouded rotors. In order to minimize the efficiency penalty, the shortest feasible axial rotor length would be desired, i.e., designs with the maximum feasible number of rotor blades.

For an analysis of the suction specific speed potential of pumps, it is sufficient to investigate only the operating regime where S^*_{max} values are to be expected. This regime can be recognized when equation (6) is introduced into equation (4) yielding

$$S^* = \frac{390}{\varphi\varepsilon\left[1+\frac{k_5\left(1+\varphi^2\varepsilon^2\right)}{\varphi^2\varepsilon^2}\right]^{3/4}} \tag{20}$$

ε = D/d denoting the rotor diameter ratio. Equation (20) reveals that an optimum value for $\varphi\varepsilon$ exists, which can be found through differentiation of equation (20) in terms of $\varphi\varepsilon$, yielding

$$(\varphi\varepsilon)_{opt} = \sqrt{\frac{k_5}{2(1+k_5)}} \tag{21}$$

Introducing now equation (21) into equation (20) gives

$$S^*_{max} = \frac{242}{\sqrt{k_5\sqrt{1+k_5}}} \tag{22}$$

indicating that the maximum obtainable suction specific speed value is a function of k_5, as graphically shown in Figure 8. If now k_5 can be interrelated with N_s and D_s, the maximum suction specific speed can be presented as function of the similarity parameters. The following considerations provide this interrelation.

Equation (21) shows that certain $\varphi\varepsilon$ values have to be maintained to operate at S^*_{max}. Since the flow factor φ is interrelated with N_s and D_s, namely

$$\varphi\varepsilon = \frac{\varepsilon^3 \, 240}{\pi^2 \, N_s^3 \, D_s^3} \left(1-\lambda^2\right)^{-2} \tag{23}$$

equation (21) also indicates that certain $N_s D_s^3$ values have to be maintained to obtain S^*_{max}. An additional relation for determining S^*_{max} is obtained by considering that the produced pump head, expressed by the head coefficient, follows the relation (no preswirl assumed)

$$q_{ad} = \eta_h \left(1 - \varphi \cot\beta_2\right) \tag{24}$$

and that

$$tg\,\beta_2 = \frac{\varphi\varepsilon}{1-\kappa} \tag{25}$$

with

$$\kappa = \frac{\Delta_{w\,u-1}}{u_1} \tag{26}$$

Subscript 1 in equation (26) refers to the inducer tip in centrifugal pumps. With this notation equation (20) to (26) are valid for axial ($\varepsilon = 1$) and centrifugal ($\varepsilon > 1$) pumps as long as the rotor blade exit angle in centrifugal pumps is equal to the inducer exit angle. Introducing equation (25) and (26) into equation (24) and considering additionally that the inducer tip inlet angle is

$$tg\,\beta_1 = \varphi\varepsilon \tag{27}$$

the head coefficient can also be expressed by the relation

$$q_{ad} = \eta_h \left(1 - \frac{1-\kappa}{\varepsilon}\right) \tag{28}$$

Since the head coefficient is also interrelated with specific speed and specific diameter (equation (15)), two equations (equation (23) and equation (15) after introducing equation (28)) are available for determining N_s and D_s, yielding unique relations for numerically determining N_s and D_s, namely

$$D_s = \frac{2\varepsilon \sqrt[4]{q_{ad}}}{\sqrt{\varphi\pi}\ \sqrt[4]{g}\ \sqrt{1-\lambda^2}} = \frac{2\varepsilon \sqrt[4]{\eta_h \left(1-\frac{1-\varkappa}{\varepsilon}\right)}}{\sqrt{\varphi\pi}\ \sqrt[4]{g}\ \sqrt{1-\lambda^2}} \tag{29}$$

and

$$N_s = \frac{60^{1.5}\, g^{3/4} \sqrt{\varphi(1-\lambda^2)}}{\sqrt{240\pi}\ q_{ad}^{3/4}\ \varepsilon} = \frac{60^{1.5}\, g^{3/4} \sqrt{\varphi(1-\lambda^2)}}{\sqrt{240\pi}\ \varepsilon \left[\eta_h\left(1-\frac{1-\varkappa}{\varepsilon}\right)\right]^{3/4}} \tag{30}$$

once $\varkappa$ is determined. In order to find the appropriate x value, equation (10) is written in the form

$$\frac{\Delta w_{u-1}}{u_1} = \frac{(k_6 - 1.02)\, w_\infty}{.6\, u_1} \tag{31}$$

and k_6 replaced by the cavitation parameter k_5, using equation (7) . Introducing equation (26) into equation (31) and observing that

$$\frac{\sin^2\beta_\infty}{\sin^2\beta_1} = \frac{1+\varphi^2\varepsilon^2}{\varphi^2\varepsilon^2 + \left(1-\frac{\varkappa}{2}\right)^2} \tag{32}$$

and

$$w_\infty = \sqrt{c_{m-1}^2 + \left(u_1 - \frac{\Delta w_{u-1}}{2}\right)^2} \tag{33}$$

an interrelation between $\varkappa$, k_5 and $\varphi\varepsilon$ results, which reads

$$k_5 = \frac{.0404\left[\varphi^2\varepsilon^2 + \left(1-\frac{\varkappa}{2}\right)^2\right] + 1.224\,\varkappa\sqrt{\varphi^2\varepsilon^2 + \left(1-\frac{\varkappa}{2}\right)^2} + .36\,\varkappa^2}{1+\varphi^2\varepsilon^2} \tag{34}$$

and can be solved graphically to yield $\varkappa$ as function of k_5 (i.e., as function of S^* according to equation (22)) and $\varphi\varepsilon$. Introducing these interrelations into equations (29) and (30), the maximum suction specific speed values can be found as function of specific speed and specific diameter. Actually equation (34) need only be evaluated for $\varphi\varepsilon$ values determined by equation (21) as long as S^*_{max} values are only of interest.

Equ. (34) can be simplified to

$$K_5 = \frac{1.2\,\varkappa\sqrt{\varphi^2\varepsilon^2 + \left(1-\frac{\varkappa}{2}\right)^2} + .04\left[\varphi^2\varepsilon^2 + \left(1-\frac{\varkappa}{2}\right)^2\right]}{1+\varphi^2\varepsilon^2} \tag{35}$$

and after further simplifications to

$$\varkappa = 483 + \frac{.125\,K_5}{1+K_5} - \sqrt{.266 - .835\,K_5 + \frac{.136\,K_5 - .418\,K_5^2}{1+K_5} + \frac{.0156\,K_5^2}{(1+K_5)^2}} \tag{36}$$

after introducing equation (21).

Figure 9 shows the interrelation between $\varkappa$ and k_5 for $(\varphi\varepsilon)_{opt}$ indicating that the minimum obtainable k_5 value is .042, i.e., the maximum obtainable suction specific speed (for t/C = .01) is about 1150 (according to Figure 8), but that at this condition $\varkappa = 0$, i.e., no head is generated in axial pumps (i.e., $N_s = \infty$). With increasing $\varkappa$ values, the suction specific speed decreases and the specific speed decreases. This trend is exhibited by axial pumps ($\varepsilon = 1$) as indicated by the dotted line in Figure 1, calculated from the above relations.

In centrifugal pumps the head depends on $\varkappa$ and ε (equation (28)), so that even with small $\varkappa$ values, large heads can be produced. Thus, high suction specific speeds can be obtained at low specific speed, providing the deflection in the initial (axial) portion of the rotor blade (inducer) can be kept low. Actually an analysis of the surface velocity distribution in centrifugal and mixed flow rotor blades is difficult, due to the three dimensional flow path. The advances in potential flow theory (and boundary layer theory for predicting separation) have not progressed far enough to interrelate k_5 and $\varkappa$ in a generally valid form, although this gap may be bridged in the near future (reference 10). Thus, calculations of the suction specific speed capability will necessarily be speculative for some rotor forms.

A frequently found inducer design in centrifugal pumps requires a flow deflection of about 60° to 70° in axial direction. With this high blade loading, flow separation is bound to occur, meaning that potential flow considerations have no validity. The published experimental information implies that k_5 values of .2 to .3 (actually an extrapolation of potential flow considerations would indicate larger k_5 values) occur in these designs, indicating suction specific speeds of $S^* = 300$ to 400. By using "backward curved" radial blades in centrifugal compressors, a considerably smaller deflection in the axial inducer becomes feasible, although the transition zone between inducer and radial portion of the blade will be more difficult to manufacture.

Assuming now that the lowest surface pressure occurs in the axial portion of the inducer and that this can be achieved by selecting a rotor blade exit angle β_2 equal to the inducer exit angle, the interrelation between $\varkappa$, k_5, β_2 and ε follows equation (25) and (34), yielding suction specific speed values as shown in Figure 10 after observing the interrelation between ε, N_s and D_s derived from efficiency considerations (Figure 3). This diagram indicates that high suction specific speeds can be obtained with centrifugal pumps when the rotor vane can be formed in such a manner that high surface velocities can be avoided. Such vane shape will cause a comparatively long flow path and correspondingly low efficiencies. By allowing a larger deflection in the inducer, the suction specific speed is reduced, the flow path shortened and the efficiency increased.

It is interesting to note that, with proper vane contouring, suction specific speeds of 1000 can be obtained when the flow deflection in the axial plane is kept small (corresponding to $\varkappa = .015$) and when the vane contour in the radial section of the rotor, and particularly in the transition section from axial direction to radial direction, is made in such a manner that low pressure regimes are avoided. It is also apparent from Figure 10 that comparatively high efficiencies can be combined with high suction specific speeds in the medium specific speed regime. Actually the mixed flow pump would appear to offer particularly good chances to combine high efficiencies with a high suction specific speed potential. By extending the application range of mixed flow pumps beyond $N_s = 300$ (this limit was calculated for geometries optimized for

efficiency) or by considering more sophisticated blade shapes (e.g. unloading the tip section at pump inlet as indicated in reference 11) for axial pumps, it appears reasonable to assume that suction specific speeds of $S^* = 1000$ can be obtained for the whole specific speed regime of centrifugal, mixed flow and axial pumps. Figure 10⊛ shows the estimated lines of constant suction specific speeds for conventional pumps, indicating that the maximum suction specific speed regime coincides with the maximum efficiency regime only for medium specific speeds.

It is important to note that the calculated S^* values are based on a chord thickness ratio of $t/C = .01$, and that larger k_5 values for equal χ values result for $t/C > .01$, i.e., lower suction specific speeds for higher chord thickness ratios. Likewise it has to be remembered that the application of preswirl is likely to increase the suction specific speed (see reference 3) and that the application of jet pumps (in front of centrifugal pumps) increases the suction specific speed of the pump assembly (reference 12). Both measures will tend to decrease the efficiency of the pump unit, indicating that a certain trade-off between suction specific speed and efficiency is possible. A more detailed discussion of these aspects is, however, beyond the scope of this study.

⊛ The maximum suction specific speed regime shown in Figure 10 differs for $N_s < 250$ from the suction specific speed regime shown in Figure 10 of reference 3. This is due to the different assumptions regarding k_5 values. In reference 3, a comparatively high k_5 value was assumed, which corresponds to designs which show a comparatively large deflection in the axial plane in order to afford a simpler to manufacture radial inlet section for the "main rotor".

Detailed investigations of the suction specific potential of drag pumps is difficult due to the complex flow pattern in this pump type. In general, it is found that a cavitation suppression head of $u^2/4g$ is required to avoid cavitation. With this assumption, lines of constant suction specific speeds can be plotted as function of N_s and D_s, as indicated in Figure 10, revealing S^* between 40 and 80 in the maximum efficiency regime of drag pumps. This makes it apparent that drag pumps have a comparatively low suction specific speed potential.

No test data on the suction specific speed of pitot pumps have been found in the literature. It may be attempted to calculate the probable potential by the following considerations. Two locations in the flow path of a typical pitot pump are likely to experience cavitation inception (1) the inlet section of the rotor and (2) the strut holding the pitot head. The cavitation suppression head for avoiding cavitation in the inlet section is $c_1^2/2g$ and for avoiding cavitation at the strut is $k_5 u_1^2/2g$, whereby k_5 may be estimated to be about .042 according to Figure 9 (assuming a chord thickness ratio of .01 and $\chi = 0$). Thus two suction specific speeds can be defined

$$S_1^* = \frac{N\sqrt{V_1}\,(2g)^{3/4}}{c_1^{1.5}} = \frac{N_s D_s^3\,\pi^{1.5}\,(2g)^{3/4}}{8\,\varepsilon^3} \tag{37}$$

and

$$S_2^* = \frac{N\sqrt{V_1}\,(2g)^{3/4}}{K_5^{3/4}\,u_1^{1.5}} = \frac{\varepsilon^{1.5}\,(2g)^{3/4}\,30\sqrt{240}}{\sqrt{N_s D_s^3}\;\pi^{1.5}\;K_5^{3/4}} \tag{38}$$

after observing that

$$V_1 = \sqrt{\varphi u \pi d^2/4} \tag{39}$$

and neglecting the displacement effect of the exit pipe. It is evident that S_1^* increases with increasing values of $N_s D_s^3$ values, whereas S_2^* decreases with increasing $N_s D_s^3$ values. Thus the maximum suction specific speed is found by equating equation (37) and (38) yielding $S_{max} = 3130$ and

$$\varepsilon^3 = \frac{N_s D_s^3}{197} \tag{40}$$

i.e., a relation for the optimum diameter ratio (for obtaining S^*_{max}) which is graphically presented in Figure 10 by lines of constant ε values. It thus results from these calculations that the pitot pump is likely to achieve higher suction specific speeds than other conventional pumps.

Fluid dynamic considerations on displacement pumps would lead to the conclusion that comparatively high suction specific speeds can be expected due to the comparatively low flow velocities in the flow path. The high pressure loading on the vanes or on the piston, however, in many designs causes clearance cavitation, thus limiting the obtainable suction specific speed. A more detailed discussion of the cavitation behavior of displacement pumps would exceed the scope of this study, so that no generalized S^* values are presented for this pump type.

Design Point Performance of Shear Force Pumps

Efficiency Relations

An analysis of the rotor efficiency and cavitation criterion of shear force pumps is presented in references 1, 2 and 13. Figure 11 shows a comparison of tested rotor head coefficients and efficiencies with calculated data for rotor configuration "A", indicating good agreement.

The key element of the analysis is a detailed investigation of the flow mechanism between the discs leading to the derivation of an expression for the optimum spacing between the disc of the form

$$P = \frac{\delta}{2}\sqrt{\frac{\omega}{\nu}} = \frac{\pi}{2} \qquad (41)$$

ω denoting the angular velocity. Accounting for the frictional losses within the rotor passage, the rotor head coefficient can be calculated as function of the flow factor φ_o (equation (46)) and rotor diameter ratio ε. This interrelation has been presented in reference 1 and may be denoted as $q_{th} - q_{fr}$ when q_{th} is defined as the ratio of the theoretically transmitted head to the reference velocity u^2/g and when q_{fr} denotes the ratio of the frictional head loss in the rotor and the reference velocity u^2/g. This interrelation is shown in Figure 12 for different diameter ratios, indicating that the head coefficient is highest at shutoff and decreases gradually with increasing flow factors. It is also evident from this diagram that the flow factor has comparatively small values. Realizing now that the difference between wheel speed and peripheral flow velocity at rotor exit is comparatively small (low slip), Figure 13, it becomes evident that the flow angle at disc exit is exceedingly small, namely, between $1/4^\circ$ and 5°, as shown in Figure 14. Thus the absolute

velocity c_2 at rotor exit is about equal to the wheel speed, meaning that about half of the energy transmitted to the fluid exists in the form of kinetic energy at rotor exit. Thus the degree of reaction is 50% (or larger). Hence c_2 has to be decelerated efficiently in order to obtain high pump efficiencies.

Several rotor-diffuser combinations are feasible. In order to recognize significant trends, a rotor-diffuser arrangement where the diffuser section consists of a vaneless (or vane type) diffuser, followed by a collector scroll, Figure 11B, may be analyzed. Treating the vaneless parallel walled diffuser on a somewhat simplified basis, the head loss can be expressed by the relation

$$H_{Lost} = \frac{c^2}{2g} \frac{L}{D^*} \frac{.316}{\sqrt[4]{Re}} \tag{42}$$

The flow path length L (logarithmic spiral) may be approximated by

$$L = \frac{(\mu - 1) D}{2 \sin \alpha_2} \tag{43}$$

with μ denoting the diameter ratio of the vaneless diffuser and α_2 the flow angle. The hydraulic diameter D^* in equation (43) becomes 2b for the vaneless diffuser, b denoting the diffuser width. Assuming for the velocity head an average value of

$$c^2 = \frac{c_2^2 + c_3^2}{2} \tag{44}$$

c_3 denoting the diffuser exit velocity, equation (43) simplifies to

$$\frac{H_{Lost}\, 2g}{u^2} = \frac{(\mu - 1)\left(1 + \frac{1}{\mu^2}\right)}{30 \sqrt[4]{Re^*}\ \varphi_0 y (\ell/D)^{1.25}} \tag{45}$$

when the channel Reynolds R_e in equation (42) is replaced by the machine Reynolds Number R_e^*, when ℓ denotes the rotor length and y the difference between free meridional flow area in the rotor and free meridional flow area

in the stator, a parameter which usually assumes values of .5 due to the necessity of selecting the disc width equal to δ . Additionally, $c_2 = u_2$ and $\sin \alpha_2 = \varphi_o$ was assumed, as justified by the low slip and shallow flow angle, when

$$\varphi_o = \frac{c_{m\text{-}2}}{u_2} \tag{46}$$

denotes the rotor exit flow factor.

Equation (45) is graphically presented in Figure 15 for several μ values and indicates extremely high losses when large diameter ratios are selected. The reason for the high loss is the large flow lengths in a parallel walled diffuser at small flow factors (logarithmic spiral flow path). It would appear that this could be modified by converging the side walls, thus increasing the meridional flow component and thereby decreasing the flow lengths, which would imply a reduced head loss. In doing so, the hydraulic diameter is decreased so that the product $\varphi_o \, l/D$ stays constant (equation (45)) and the head loss would tend to remain about constant. This is a somewhat pessimistic appraisal, since actually the meridional flow acceleration reduces the tendency to flow separation, so that a small reduction in losses may be expected with converging side walls. It is apparent, however, from Figure 15, that only a comparatively small μ value should be selected. This means that the diffusion rate is small, so that an additional diffusing element, e.g., a vane type diffuser, must be provided.

The absolute low angle α_2 in the diffuser can be increased by converging the meridional flow path as schematically indicated in Figure 11 "A". With this rotor design concept, an additional frictional area (F in Figure 11 "A") is created, which will cause windage losses at the outer shroud surface. The magnitude of this loss can be expressed by the relation

$$\frac{H_{sh}\, 2g}{u^2} = \frac{\gamma_x}{\varphi_0 \gamma \; 10\pi \; \gamma_\ell \sqrt[5]{Re^*}} \tag{47}$$

with γ_ℓ denoting the density of the pumped liquid and γ_x denoting the density of the medium, wetting the outer shroud surface. Equation (47) is also graphically presented in Figure 15 for $\gamma_x / \gamma_\ell = 1$, indicating comparatively high loss values. This loss, however, could be almost entirely eliminated by providing an effective seal at point S in Figure 11 "A", thus allowing only ambient air to wet the shroud surface. This may, however, in many cases, be prohibitive due to the high sliding velocities at the seal surface.

Another possibility would be to provide a scroll collector directly behind the rotor, followed by a single conical diffuser. The likely losses in the collector may be calculated by using equation (42) assuming a flow path length of .5 D and a hydraulic diameter equal to half the collector exit diameter (assuming circular cross-section)

$$D^* = D\left(\varphi_0 \gamma \, {}^{\ell}/_{D} + \sqrt{\varphi_0 \gamma \, {}^{\ell}/_{D}}\right) \tag{48}$$

Thus, the collector losses may be represented by the relation

$$\frac{H_{sc}\, 2g}{u^2} = \frac{.079\,\pi}{\sqrt[4]{Re^*}\left(\varphi_0 \gamma \, {}^{\ell}/_{D} + \sqrt{\varphi_0 \gamma \, {}^{\ell}/_{D}}\right)^{1.25}} \tag{49}$$

which is also graphically shown in Figure 15. Comparing the collector losses with the shroud losses and vaneless diffuser losses (for small μ values), it results that all these losses have the same trend, namely, increasing with decreasing flow factors. Although operating regimes can be recognized in Figure 15, where one arrangement is better than the other, the collector loss relation appears to represent average values and may therefore be used for the subsequent calculations.

The above considerations dealt mainly with the losses directly behind the rotor, i.e., were mainly concerned with the flow collection problem. Additionally, the subsequent diffuser losses must be considered. They may be assessed by assuming a single conical diffuser. Loss values of $H_D 2g/u^2 = .16$ to $.3$ result for this arrangement from reference 15 for diffusion rates between 5 and 15.

In order to complete the fluid friction loss considerations, the rotor inlet losses have to be calculated, which, by using equation (10) of reference 1, can be expressed by the relation

$$\frac{H_{in}\, 2g}{u^2} = 16\, \varepsilon^4 \left(\varphi_0 \gamma\, {}^{l}/_{D}\right)^2 \qquad (50)$$

Figure 16 shows the collector-diffuser losses and inlet losses graphically for an assumed value of $H_D 2g/u^2 = .3$, indicating that these losses become a minimum at $\varphi_0 \gamma\, {}^{l}/_{D}$ values of .003 to .01.

Considering that the pump head coefficient is

$$q_{ad} = \frac{H_{ad}\, g}{u^2} = q_{th} - q_{fr} - \frac{H_{sc} + H_D + H_{in}}{u^2/g} \tag{51}$$

its numerical value can be calculated from Figures 12 and 16, yielding values shown in Figure 17, indicating maximum head coefficients at low flow factors.

In order to calculate the pump efficiency, the windage losses at the rotor end discs have to be considered, which can be calculated by the relation (neglecting slip)

$$\frac{H_W\, 2g}{u^2} = \frac{.01}{\varphi_0 \gamma\, \ell/D\, \pi\, \sqrt[5]{Re^*}} \tag{52}$$

Thus, the pump efficiency becomes

$$\eta = \frac{q_{ad}}{\frac{c_u}{u} + \frac{H_W g}{u^2}} \tag{53}$$

graphically shown in Figure 18, and indicating maximum efficiency values of .55.

It is important to realize that the losses discussed above depend on the Reynolds Number and are quoted in terms of the machine Reynolds Number R_e^*, and that the rotor performance calculations are only valid for laminar flow within the rotor. In order to insure laminar flow in the rotor, the rotor inlet Reynolds Number should be below 2000 when the inlet Reynolds Number is defined by

$$Re\text{-}r = \frac{c_r\, \delta\, 2}{\nu} \tag{54}$$

c_r denoting the radial velocity component at disc inlet.

By observing equation (41), an interrelation between machine Reynolds Number and rotor inlet Reynolds Number can be derived, which reads

$$Re_r = \frac{2 \varphi_0 \pi \sqrt{Re^*}}{\sqrt{2}} \tag{55}$$

Introducing equation (57) into equation (55), the rotor inlet Reynolds Number can be expressed as function of N_s. This leads to Figure 19, indicating that the maximum permissible machine Reynolds Number becomes about 2×10^6 for large diameter ratios, and up to 10^9 for small diameter ratios. Thus the typical Reynolds Number regime of conventional pumps can also be covered by shear force pumps.

Another point of interest is the Reynolds Number in the diffuser section, which is interrelated with the machine Reynolds Number by

$$Re_D = 2 Re^* \left(\varphi_0 \psi \, {}^{l}/_{D} + \sqrt{\varphi_0 \psi \, {}^{l}/_{D}} \right) \tag{56}$$

and graphically presented in Figure 19. It becomes evident that the machine Reynolds Number is restricted to $R_e^* > 10^5$ for operation at low specific speeds in order to maintain reasonably high diffuser Reynolds Number.

The design performance characteristic of shear force pumps can now be generalized by presenting the efficiency in terms of the similarity parameters. Using the interrelation

$$N_s = \frac{60 \, g^{3/4} \sqrt{\varphi_0 \psi \, {}^{l}/_{D}}}{\sqrt{\pi} \, q_{od}^{3/4}} \tag{57}$$

and

$$D_s = \frac{q_{od}^{1/4}}{\sqrt{\pi}\, g^{1/4} \sqrt{\varphi_o y \ell/D}} \qquad (58)$$

Figure 20 is computed, indicating highest efficiencies at specific speeds between 30 and 40, and decreasing with lower specific speeds namely to about 20% at specific speeds of 17. The specific diameters are of similar magnitude as the specific diameters of conventional pumps.

It is interesting to note that the "rotor head coefficient" depends mainly on the flow factor φ_o and the diameter ratio (Figure 12), whereas diffuser losses, inlet losses and windage losses depend on the flow factor, diameter ratio and rotor length ratio $y\ \ell/D$ (equations (49), (50) and (52)). This suggests that an optimum value of $y\ \ell/D$ exists for obtaining maximum efficiencies. In order to determine this value, $N_s D_s$ diagrams for several $y\ \ell/D$ values were calculated. These computations indicated that a $y\ \ell/D$ value of about .25 gave highest efficiencies over the investigated specific speed range. Hence, the $y\ \ell/D$ value in Figure 20 is assumed $y\ \ell/D$ = constant = .25.

It would be premature to consider the efficiency data shown in Figure 20 as maximum obtainable values, since the assumptions regarding diffuser performance are necessarily speculative. It appears feasible to assume that lower diffuser losses than presented in Figure 16 can be obtained with further development efforts. A promising concept is sketched in Figure 21. The fluid discharged from the rotor is accelerated in its meridional flow path and discharged to the

side with the wheel shroud rotating in ambient air rather than be wetted by the pumped fluid. This design would favor a radial inward diffuser and collection of the pressurized fluid in the center. This concept is similar to the one conventionally applied for pitot pumps. The friction of the outer shroud becomes negligible, assuming that the density difference in the fluid and ambient is larger than 800, and the main development problem would be that of designing a diffuser having efficient recovery with inward flow. It becomes apparent that the flow has to be turned by about 90° in order to obtain maximum deceleration. Slotted vanes to avoid excessive boundary layer growth (reference 14) and excessive blade loading would appear to offer the possibility of obtaining higher than usual efficiencies. Actually the slotted vane concept is not limited to inward diffusers. It appears feasible to assume that a vane type diffuser, following a small vaneless diffuser in an arrangement shown in Figure 11, may also yield somewhat higher diffuser efficiencies $\left(H_D 2g/u^2 < .3\right)$ than assumed sofar. With a successful development of efficient diffusers, peak efficiencies of about 60% at specific speeds of 40 and efficiencies of about 20% could be realized at specific speeds of 6 .

Suction Specific Speed Relations

Due to the working mechanism in the rotor, no regime of low blade surface pressures exist within the rotor, meaning that the fluid pressure rises as soon as the flow enters the rotor. Thus the minimum static pressure occurring in the flow path is the static pressure at pump inlet. Hence, the cavitation suppression head can be represented by the equation

$$H_s = \frac{c_i^2}{2g} \qquad (59)$$

when c_1 denotes the inlet velocity. Introducing now equation (59) into equation (4), it results for the suction specific speed

$$S_i^* = \frac{(2g)^{3/4}\ 60}{\sqrt{\pi}\ 8\ \varepsilon^3\ \varphi_0\ y\ \ell/D} \tag{60}$$

In equation (60) the axial inlet velocity was used as cavitation criterion. In order to avoid low pressure regimes at rotor entrance, the radial inflow velocity c_r should not be larger than c_1. A suction specific speed, based on c_r follows the relation

$$S_r^* = \frac{(2g)^{3/4}\ 60\ \sqrt{y\ \ell/D}}{\sqrt{\pi}\ \varphi_0\ \varepsilon^{1.5}} \tag{61}$$

Thus

$$\frac{S_r^*}{S_a^*} = \left(4y\ \ell/D\right)^{1.5} \tag{62}$$

Since the optimum $y\ \ell/D$ value found from efficiency calculations is .25, it follows from equation (62) that $S_r^* > S_a^*$ for Figure 22, thus rendering the presented S_a^* value the limiting specific speed value.

Comparison of Design Point Performance of Shear Force Pumps and Conventional Pumps

In order to recognize the major trends in pump performance, Figure 22 is presented, which shows the maximum obtainable efficiency of conventional pumps and shear force pumps, together with the obtainable suction specific speeds for design geometries optimized for maximum efficiency. It is evident from this diagram that the shear force pump is a low to medium specific speed device, and that in

all specific speed ranges the maximum calculated shear force pump efficiency is lower than that of conventional pumps. Comparing the obtainable suction specific values (see also Figure 23), it becomes evident that the shear force pump exceeds the suction specific speeds obtainable with conventional pumps in the low to medium specific speed regime by factors exceeding 10, even when conventional pumps are credited with sophisticated design concepts.

Off-Design Performance

Typical performance characteristics of conventional pumps are shown in Figure 24 in a dimensionless form by plotting the head coefficient as function of the flow factor, together with the pump efficiency. This represents at the same time the characteristics of a pump operating at constant speed. It is evident that, at part load operation (low flow factors), a somewhat higher pressure than design pressure is usually obtained, but that at a certain minimum flow rate, instable operation (surge) is likely to occur. Figure 24 shows also that the efficiency decreases with part load operation. At volume flows higher than the design volume flow, the pressure usually decreases, together with the efficiency. A typical cavitation behavior is shown in Figure 25 by plotting the suction specific speed as function of the flow factor. This behavior follows from the cascade theory, and may be discussed as follows: A typical surface velocity distribution for design point operation was shown in Figure 2 indicating a decreased surface pressure at the suction side. If now the flow rate is changed at constant pump speed, the cascade operates under an oblique angle of attack, which causes the pressure distribution along the blade surface

to change. For part load performance, the point of minimum surface pressure still stays at the suction side but moves toward the leading edge. This causes a larger difference between static inlet pressure and suction side surface pressure. By operating the pump at overload conditions, the point of minimum pressure will occur at the pressure side due to the oblique angle of attack. This pressure for $V/V_o > 1.1$ will tend to be lower than the minimum suction side pressure at design point operation. Hence, in general, the required cavitation suppression head at off-design operation will tend to be higher than the cavitation suppression head at design point operation. This trend is graphically demonstrated in Figure 25. It may be added that, due to secondary flow phenomena in the inlet section at part load operation, a tip eddy frequently originates in the upper portion of the channel, which changes the pressure distribution at the tip section of the blade in such a manner that the critical pressure regime moves to a lower radius. Since, as indicated in Figure 7, lower cavitation suppression heads are needed at smaller radii, it is sometimes found that no increasing cavitation suppression head is required when operating at part load. Conversely, an eddy tends to establish itself at the hub section when operating at overload condition, thus exaggerating the cavitation suppression head requirement and thereby making the pump even more sensitive to cavitation when operating at overload.

The direction of the rotor inlet flow vector does not affect the pressure distribution in the rotor of a shear force pump. Only the magnitude of the meridional

velocity is responsible for the required cavitation suppression head. Thus, the required cavitation suppression head of shear force pumps decreases with decreasing volume flows and increases with increasing flow rates, as shown in Figure 26. The efficiency and pressure head generation of shear force pumps is also shown in Figure 26 as function of the flow factor, indicating that the pressure tends to rise steadily up to shutoff for designs which have a vaneless diffuser. By providing a vane type diffuser, incidence losses at the guide vane leading edge can cause a decrease in pump head at low flow factors and thus an instability regime at part load operation.

Comparing Figure 25 with Figure 26, it becomes apparent that shear force pumps have a more favorable cavitation behavior at part load operation, meaning that lower cavitation suppression heads are required if the shear force pump is operated at part load, in contrast to the cavitation characteristic of conventional pumps.

Application of Shear Force Pumps

Figure 23 shows that the outstanding feature of shear force pumps is the high suction specific speed. This means that only very small cavitation suppression heads are required, so that fluid temperatures can be tolerated which are close to the boiling temperature. Hence profitable application for this pump type are condensate pumps in Rankine cycles. In these systems the fluid leaves the condenser section in a saturated state and then passes through the sub-cooler section where the temperature is decreased below the saturation temperature. The

amount of sub-cooling depends on the required cavitation suppression head of the pump. For high suction specific speed pumps, only a comparatively small sub-cooling section is needed so that the system weight and installation envelope are reduced significantly. In contrast, the pump efficiency is usually of little consequence, since the power demand of condensate pumps is only a minor fraction of the net output. Thus it is expected that the exploitation of the unique features of shear force pumps will contribute significantly to the design of more compact space power systems with improved specific weight factors.

Typical pump requirements for solar space powerplants are listed in Table I[*] for three different fluids. Assuming that the pumps are to run with the same speed as the power turbine, specific speeds between 25 and 62 result, i.e., values which are in the best efficiency regime of shear force pumps.

Conclusions and Recommendations

Shear force pumps will, in general, show considerably higher suction specific speeds than conventional pumps, even if sophisticated blade design concepts are utilized for cavitation suppression in conventional pumps. At part load performance, shear force pumps need a smaller cavitation suppression head than at design

[*] Communication from Mr. F. R. Ostiek, Flight Accessory Laboratory, Aeronautical Systems Division, WPAFB.

point, in constrast to the part load behavior of conventional pumps where larger cavitation suppression heads are required at part load. The efficiency of well developed shear force pumps will tend to be lower at design point as well as part load operation than conventional pumps. Peak efficiencies of about 55% are calculated, occurring in specific speed regimes of 30 and 40. It is likely that higher efficiencies, up to 65%, can be obtained with refined diffuser designs.

The tested rotor performance is in good agreement with the calculated data, indicating that the rotor flow theory is sufficiently well developed. Lacking, However, are data on the diffuser performance. Since shear force pumps are 50% reaction machines, efficient diffuser designs have to be established before applications of shear force pumps can be contemplated.

Unique requirements are imposed on the diffuser design due to the shallow rotor flow discharge angle. An experimental development program is considered to be the most effective approach for meeting these requirements efficiently.

The outstanding suction specific speed characteristic of shear force pumps can be utilized advantageously in the design of lightweight compact space powerplants of the Rankine cycle type, since the low cavitation sensitivity will contribute significantly to a reduction in weight and size of the sub-cooler section. It is therefore recommended that development work be initiated for experimental designs of efficient shear force pump diffusers.

REFERENCES

1.	S. H. Hasinger L. G. Kehrt	"Investigations of a Shear Force Pump" ASME Transactions, Engineering for Power, July 1963
2.0	O. T. Goksel S. H. Hasinger L. G. Kehrt	"Cavitation Tests with a High Efficiency Shear Force Pump" - ARL Report (Submitted to ASME for presentation as a paper)
3.	O. E. Balje	"A Study on Design Criteria and Matching of Turbomachines" - ASME Paper 60-WA-231
4.	J. Speeds	"Study, Design and Test of Experimental Liquid Hydrogen Pump for Use in Flight Vehicles Systems" ASD-TDR-63-114, February 1963 Contract AF33(657)-8062
5.	K. E. Nichols D. G. McPherson O. E. Balje	"Study of Turbine and Turbopump Design Parameters" S/TD No. 1735, Department of the Navy, Office of Naval Research, Contract No. NONR 2292(00) - Task No. NR094-343
6.	G. L. Mellor	"An Analysis of Axial Compressor Cascade Aerodynamics" ASME Transactions, Basic Engineering - September 1959
7.	R. D. Bowerman	"The Design of Axial Flow Pumps" ASME Transactions, November 1956
8.	G. M. Wood	"Visual Cavitation Studies of Mixed Flow Impellers" ASME Paper 62-Hyd-12
9.	W. S. Gearhart	"Tip Clearance Flow in Turbomachines" AD-605514, File No. TM506.2491-04 Contract NOw 63-0209-C - Pennsylvania State University
10.	M. J. Schilhansl	"Three Dimensional Theory of Incompressible and Inviscid Flow through Mixed Flow Turbomachines" ASME Paper 64-WA-GTP-1
11.	W. I. Chapman	"Chrysler's Gas Turbine Car, Powerplant Design Characteristic" - SAE Paper 777B, January 1964
12.	T. A. Carter C. R. Crusan	"Design Study of Liquid Oxygen Pumping Systems for Missile Fueling Incorporating Vented Storage Tanks" Advances in Cryogenic Engineering, Vol. 4 - 1960

13. M. C. Breiter, K. Pohlhausen — "Laminar Flow Between Two Rotating Discs" Report No. ARL 62-318

14. M. Schilhansl, Marcinowski — "Measurements on Axial Cascades for Decelerated Flow" (In German) Report VL 13105, March 1946

15. S. J. Kline — "Optimum Design of Straight Walled Diffusers" ASME Transactions, Basic Engineering, September 1959

NOMENCLATURE

b	Diffuser width
C	Chord length
C_L	Lift coefficient
c	Absolute velocity
D	Rotor diameter
D^*	Hydraulic diameter
D_s	Specific diameter
d	Inducer tip diameter of conventional pumps Inlet diameter of shear force rotors
d_h	Hub diameter
g	Gravitational constant
H_{ad}	Adiabatic head
H_{lost}	Head loss
k_5, k_6	Cavitation parameter
L	Flow path length
ℓ	Rotor length
m	Slip coefficient
N	Rotational speed
N_s	Specific speed
P	Pohlhausen parameter
P	Pressure
η_{ad}	Head coefficient
R	Radius ratio
R_e	Channel Reynolds Number

t	Maximum chord thickness
R_e^*	Machine Reynolds Number
r	Radius
S^*	Suction specific speed
S^*	Stroke
s	Clearance
u	Peripheral speed
V	Volume flow
W	Relative velocity
x	Deflection parameter
x^*	Fraction of chord length
y	Ratio of free meridional flow area in rotor and free meridional flow area in diffuser
α	Absolute flow angle
β	Relative flow angle, rotor angle
γ	Density
Δ	Difference, bore diameter of pitot head
δ	Distance between discs in shear force rotor
ε	Rotor diameter ratio D/d
η	Efficiency
η_h	Hydraulic efficiency
λ	Hub ratio d_h/d
μ	Diffuser diameter ratio
ν	Kinematic viscosity
φ	Flow factor
ω	Angular velocity

Subscripts

1	Rotor inlet
2	Rotor exit, diffuser inlet
3	Diffuser exit
∞	Average
b	Blade
D	Diffuser
i	Inlet
m	Meridional
sc	Scroll
sh	Shroud
u	Peripheral
W	Wheel disc

	Water	Diphenal	Mercury	
P_1	30	3	4	psia
P_3	240	100	250	psia
V	.00523	.0103	.00086	ft^3/sec
$N_{turbine}$	35,000	35,000	35,000	rpm
N_s	25	55	62.5	—

TABLE I - Typical Pump Requirements for 20KW Solar Space Power Systems

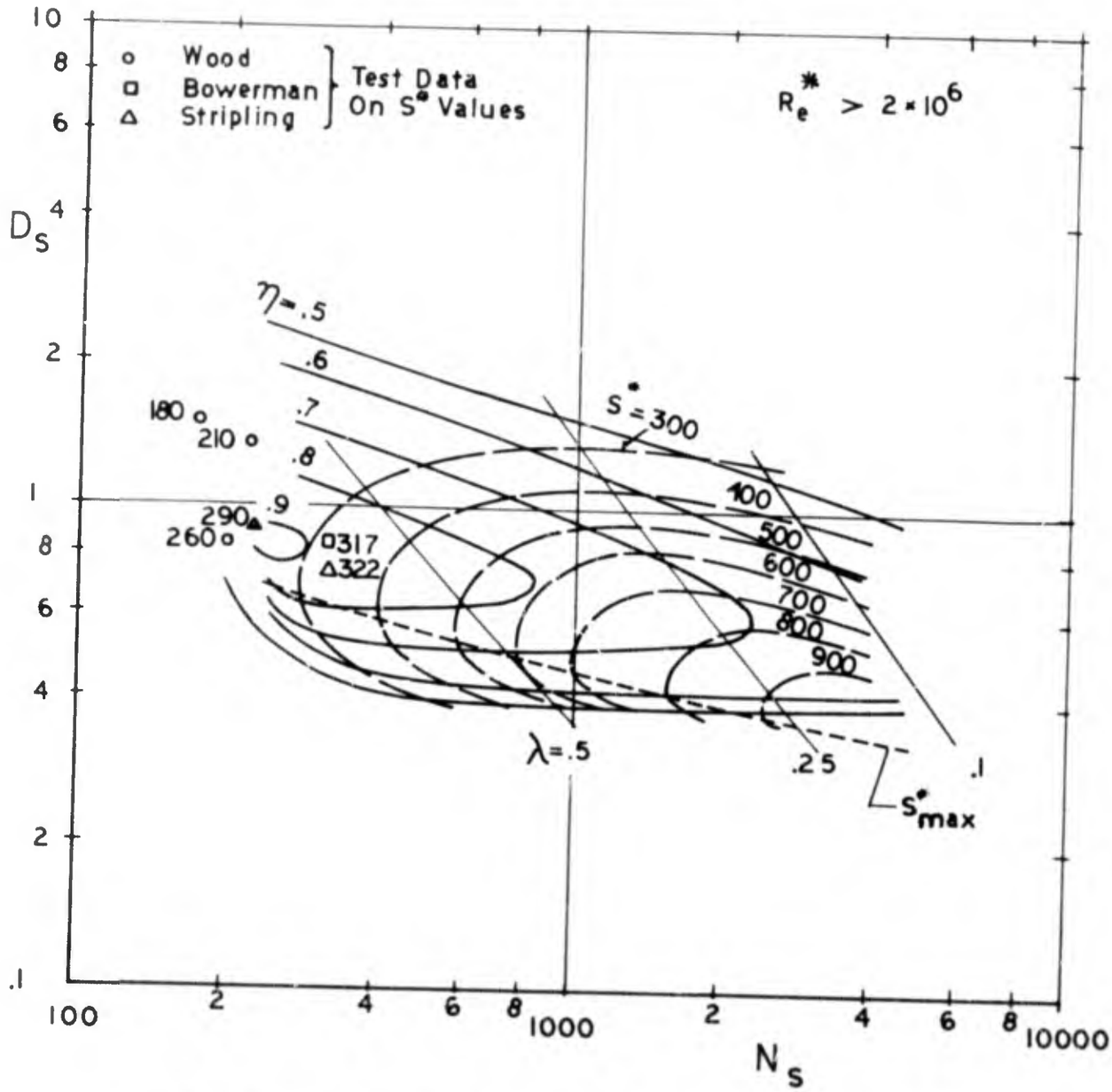

Figure 1. Typical $N_s D_s$ Diagram for Single Stage Axial Pumps

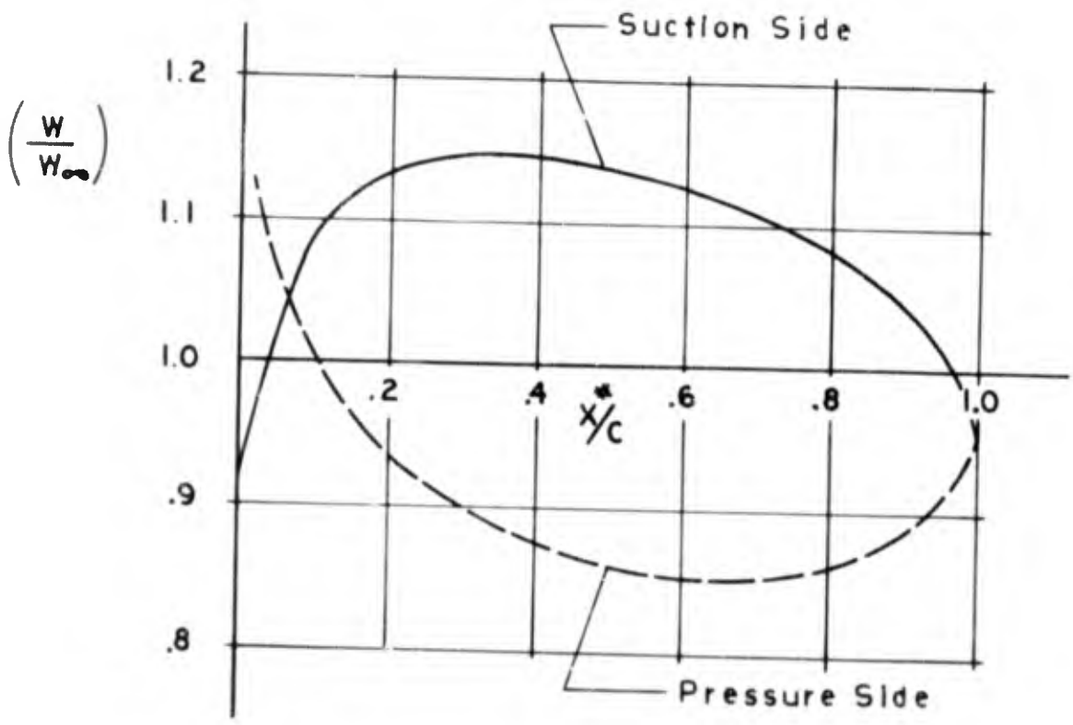

Figure 2. Blade Surface Velocity Distribution

Figure 3. $N_s D_s$ Diagram for

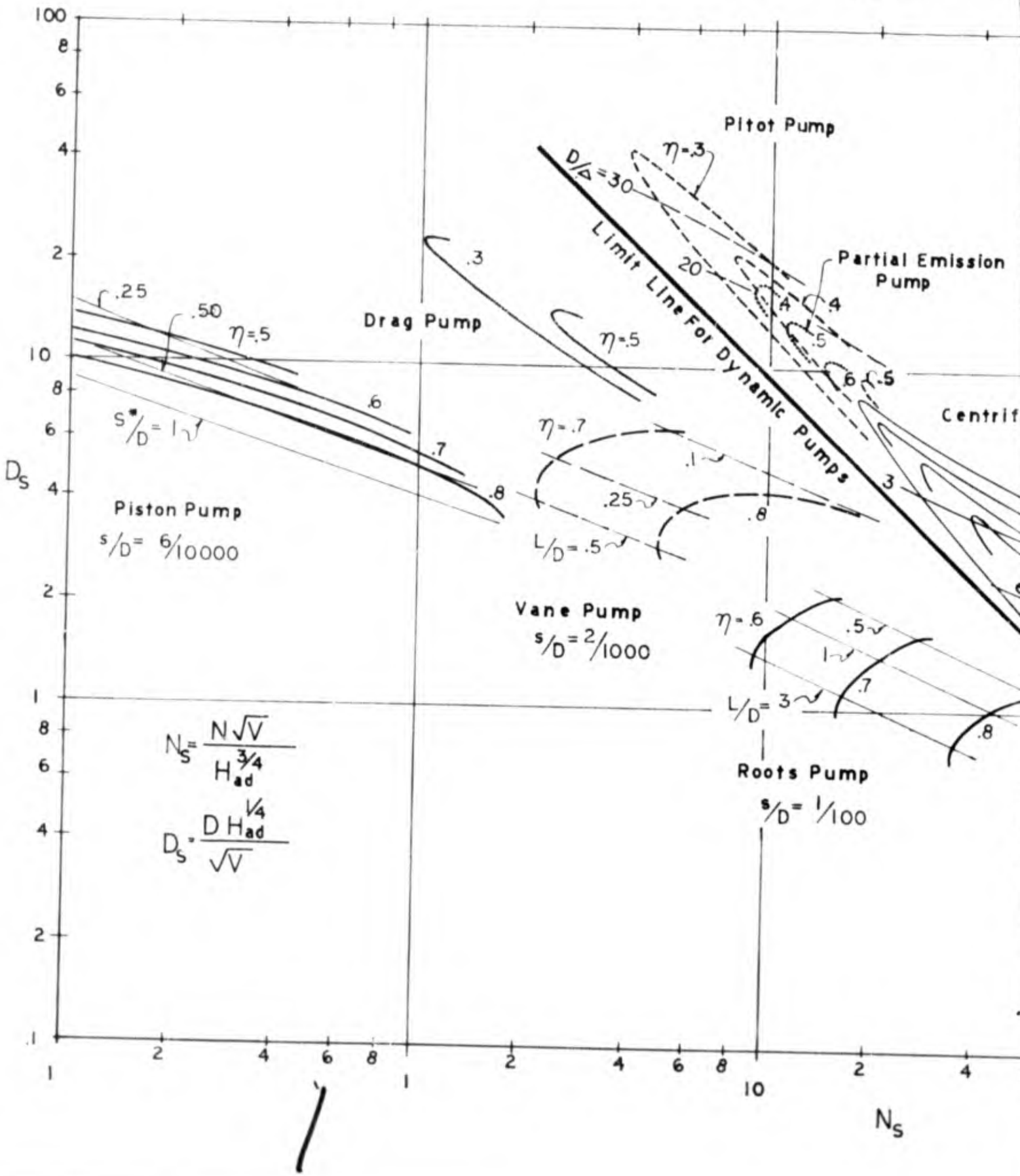

gure 3 $N_s D_s$ Diagram for Single Stage Pumps

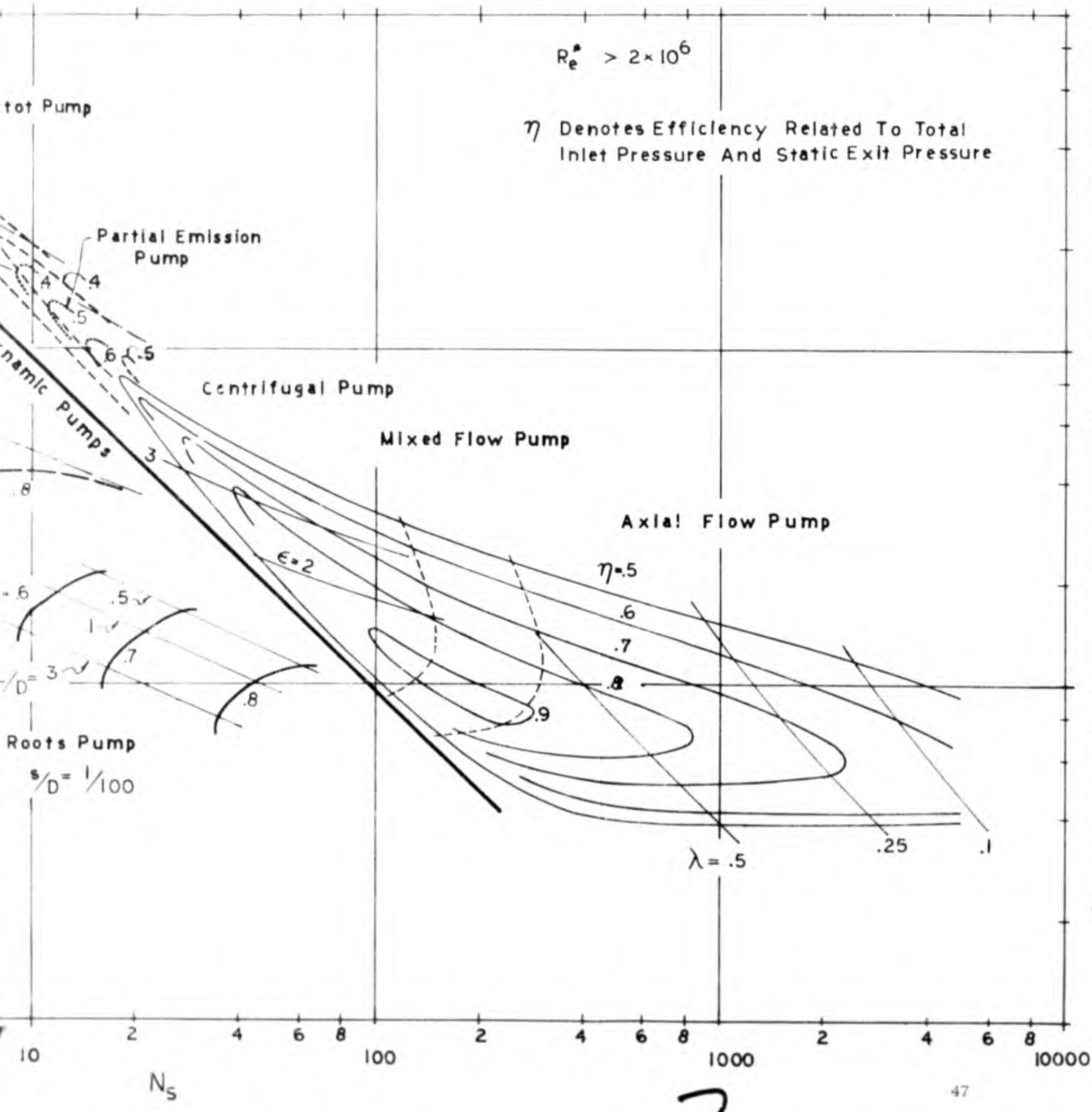

2

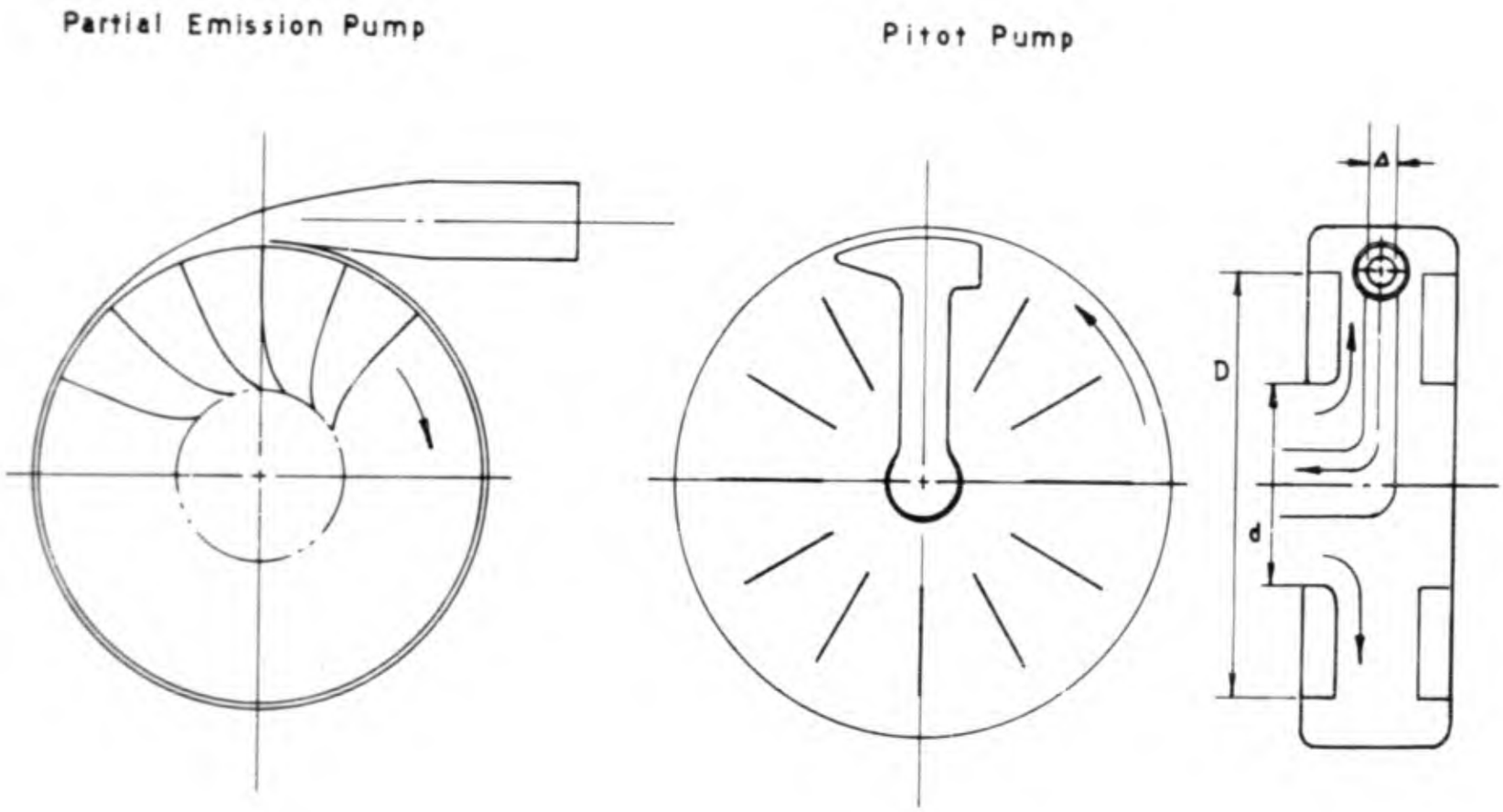

Figure 4. Schematic of Partial Emission and Pitot Pumps

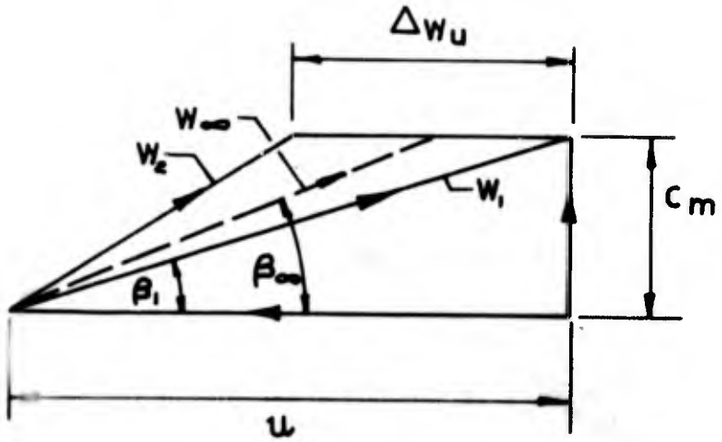

Figure 5. Velocity Triangles

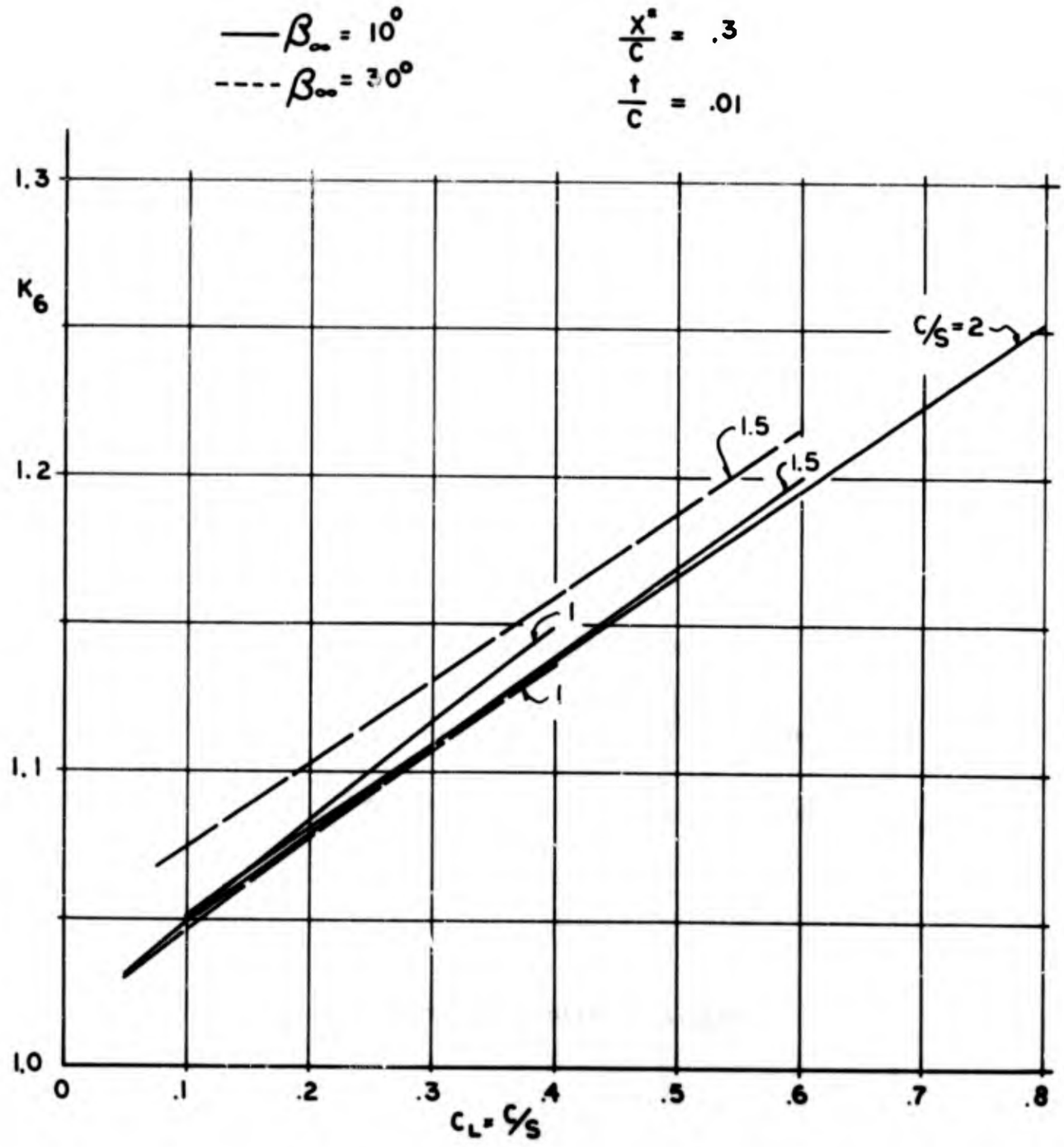

Figure 6. Cavitation Parameter k_6 as Function of Blade Parameters

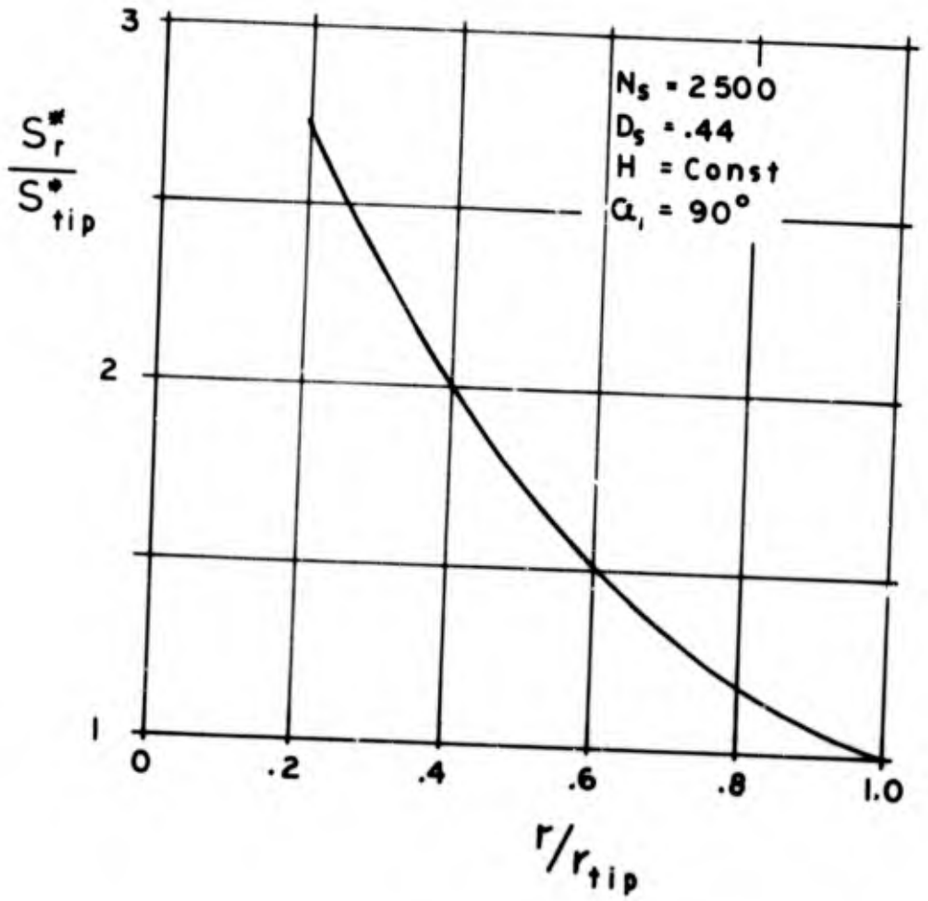

Figure 7. Suction Specific Speed as Function of Radius Ratio

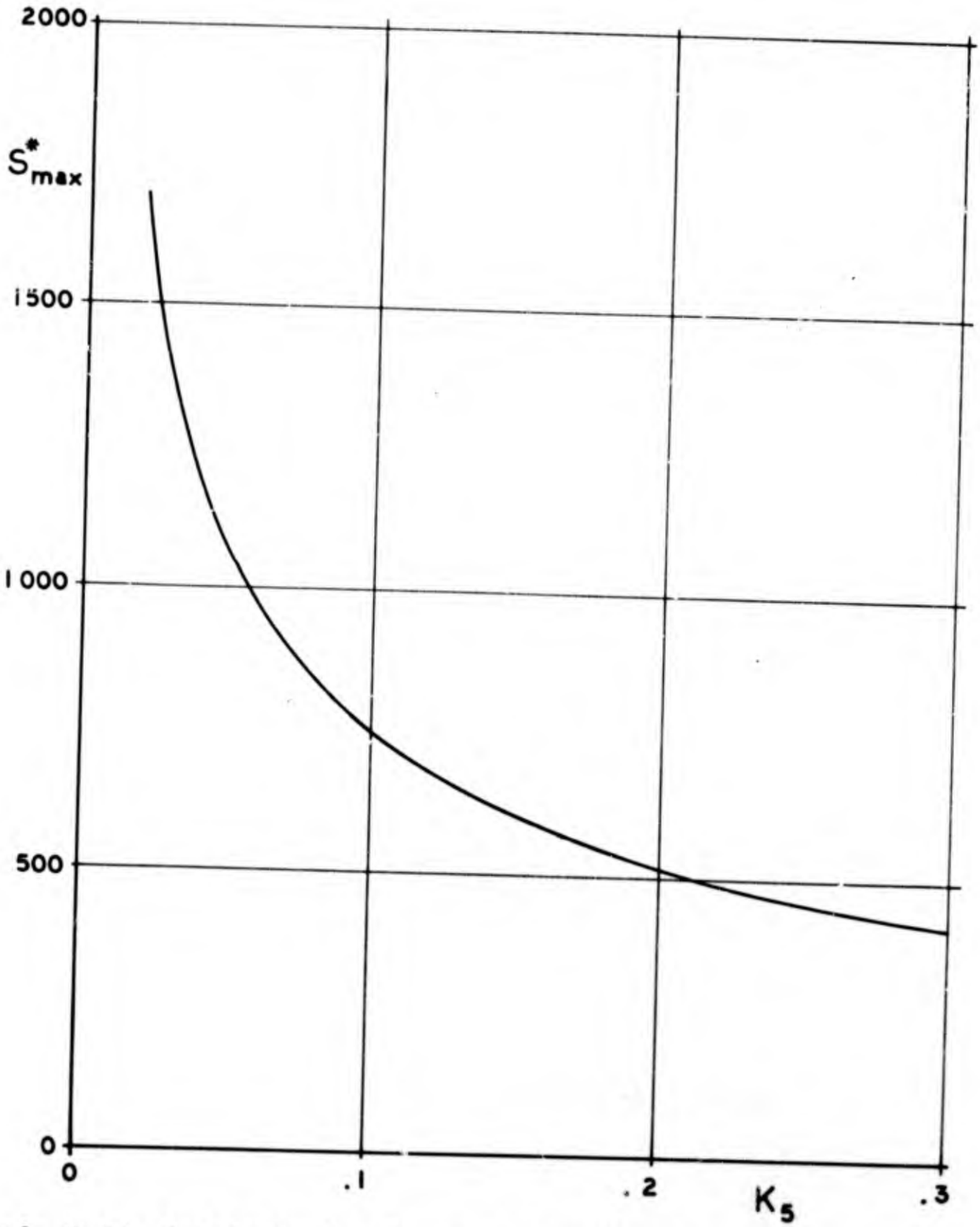

Figure 8. Suction Specific Speed as Function of Cavitation Parameter k_5

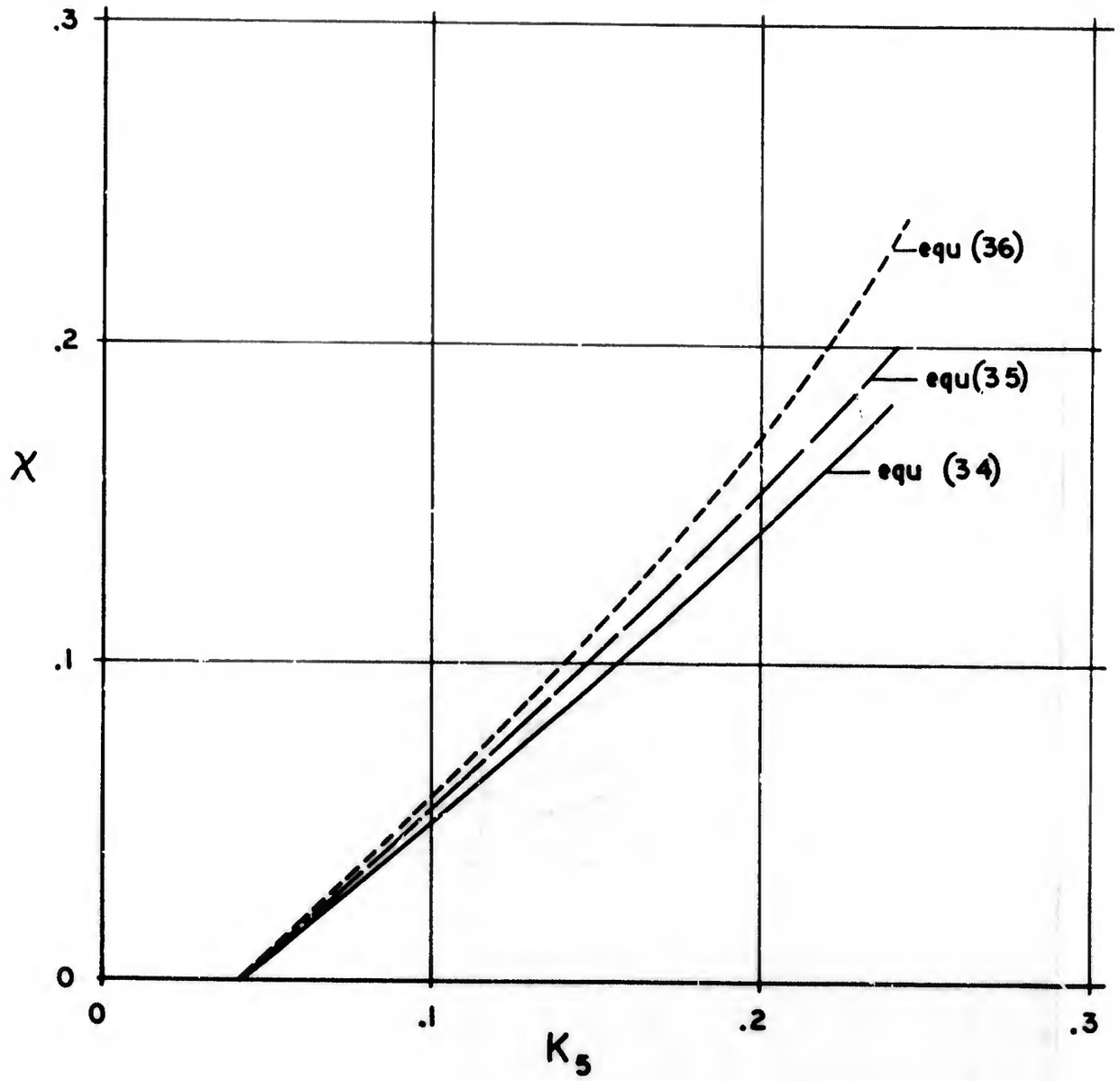

Figure 9. Deflection Parameter χ as Function of Cavitation Parameter k_5

Figure 10. Calculated Suction Specific Speed

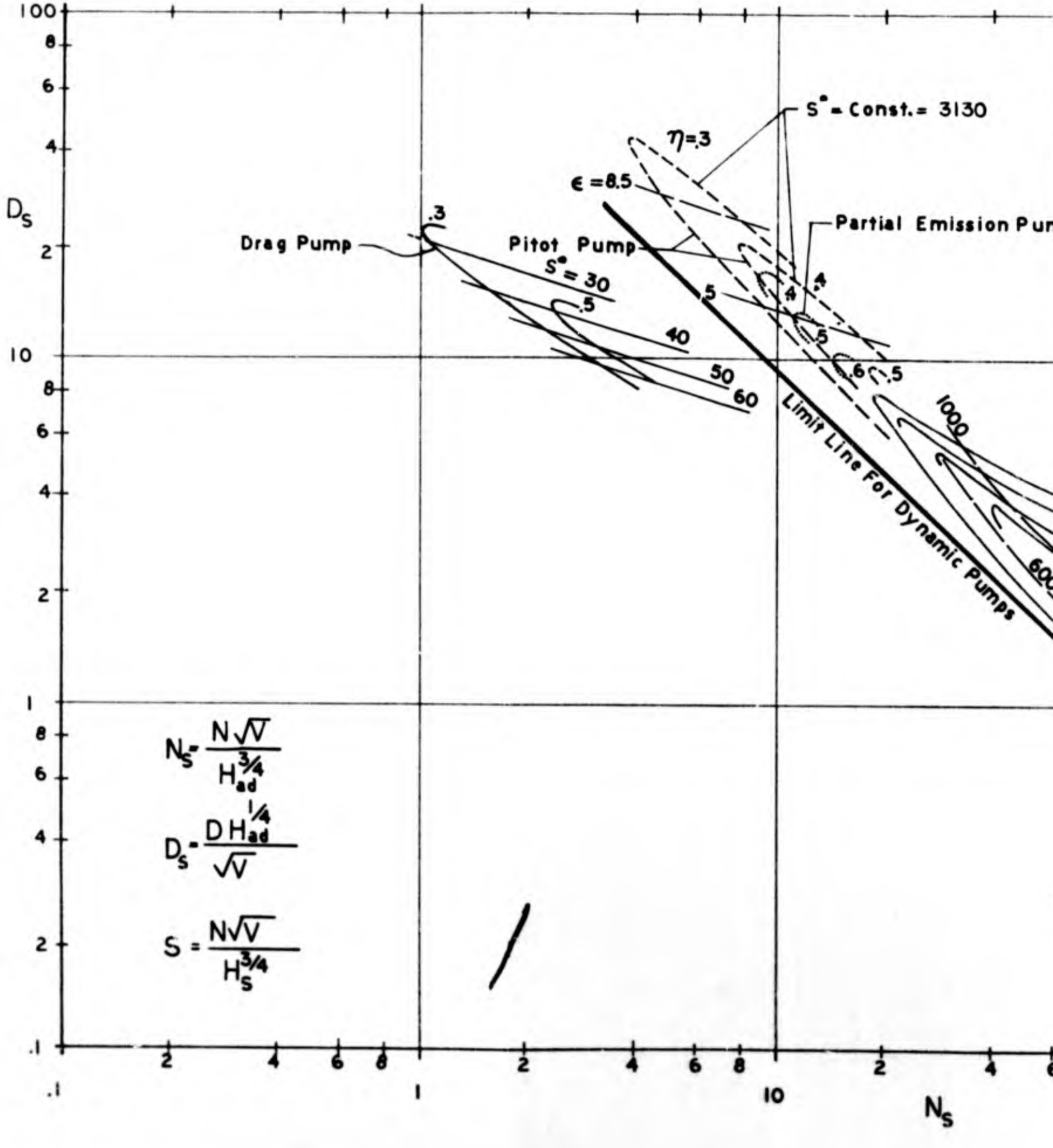

Suction Specific Speed Data for Conventional Pumps

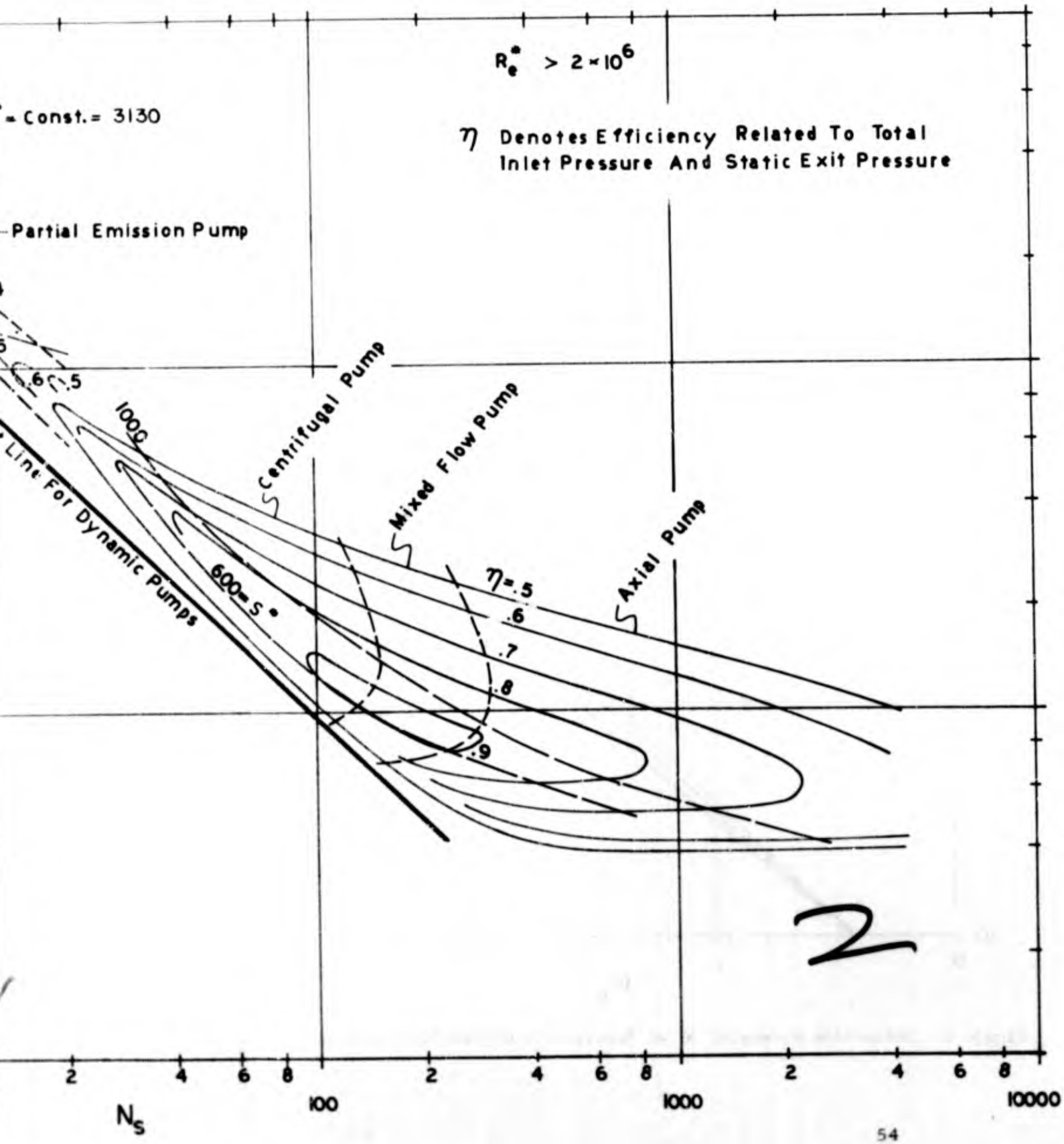

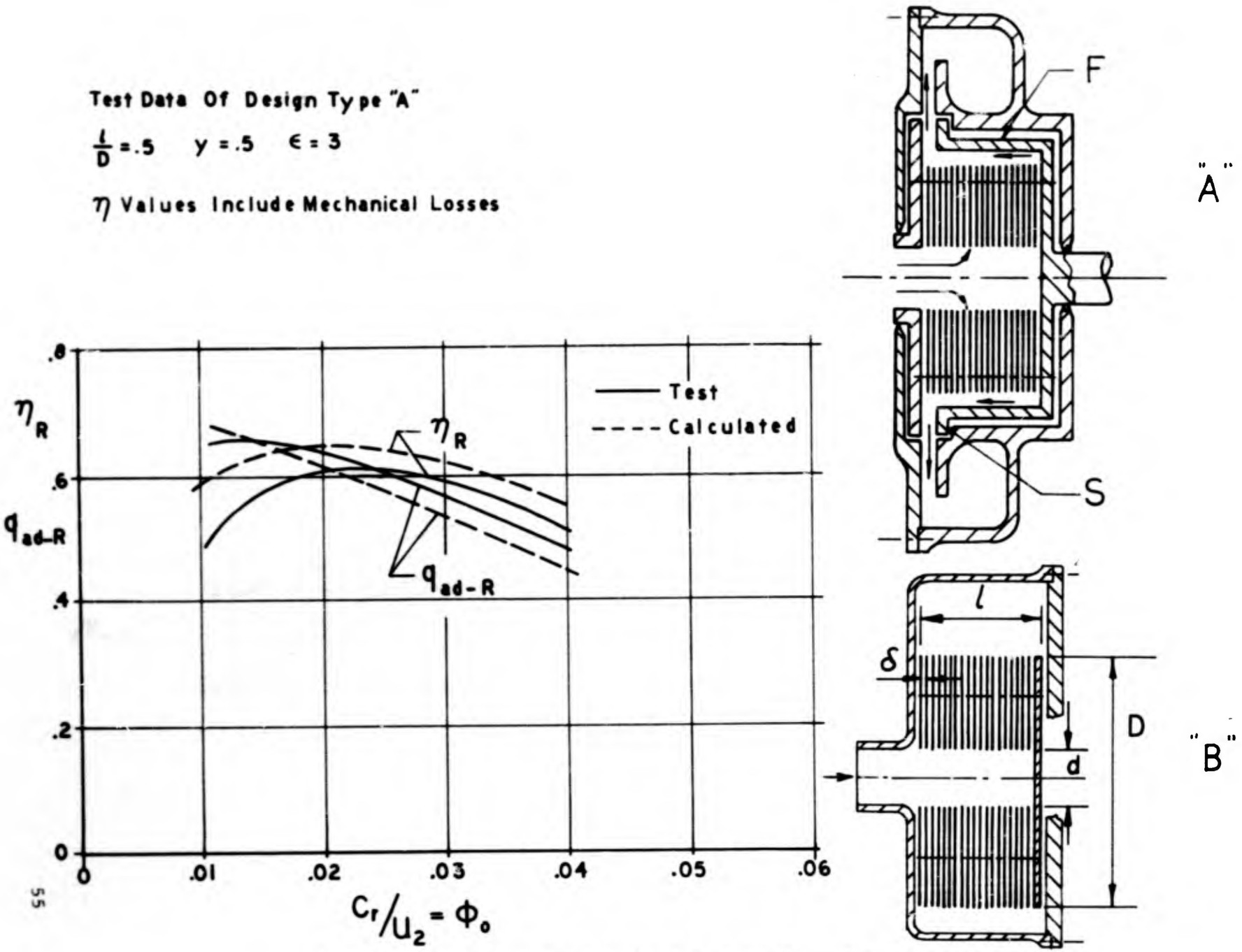

Figure 11. Schematic of Shear Force Pump and Rotor Test Data

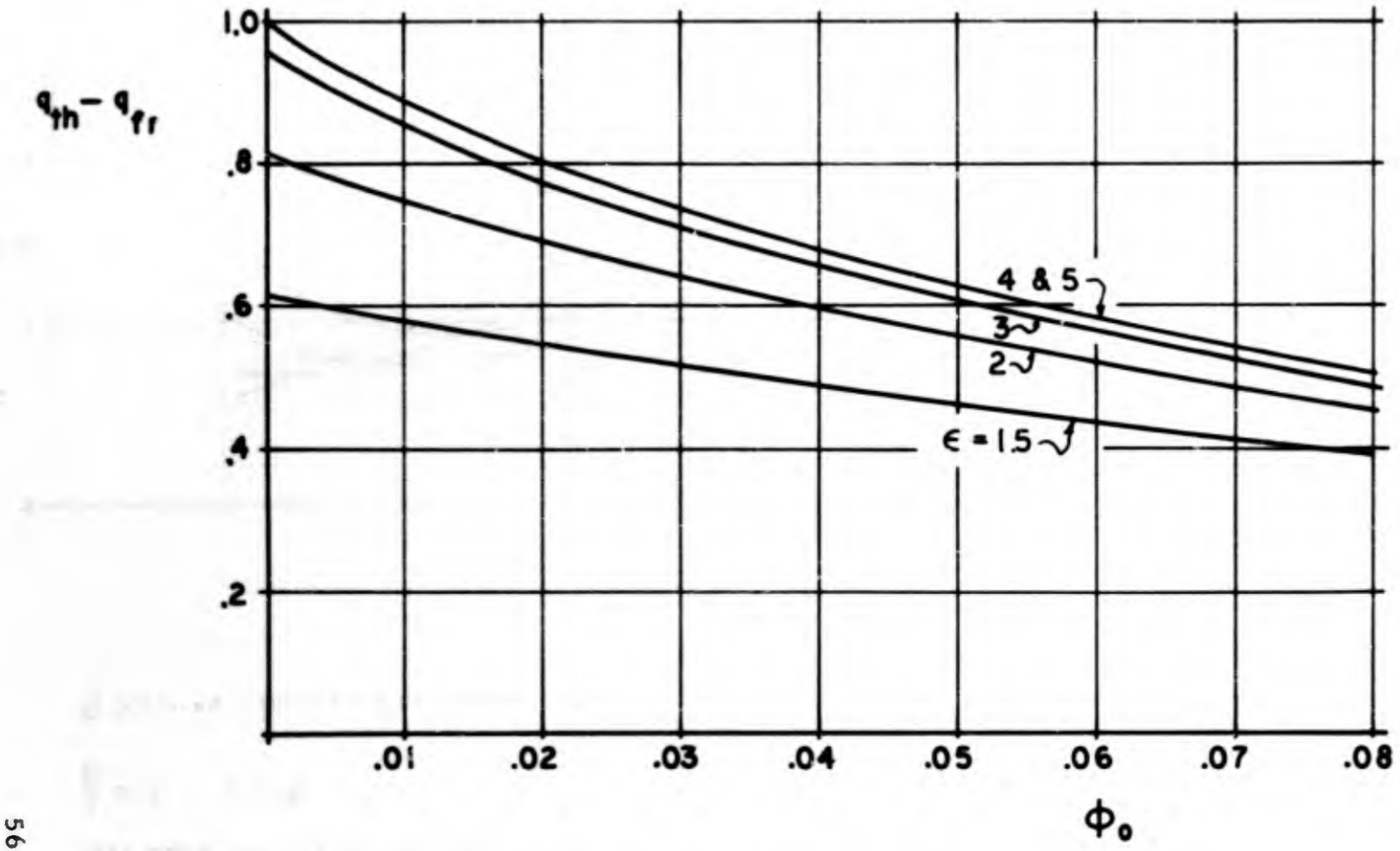

Figure 12. "Total" Rotor Head Coefficient of Shear Force Rotor

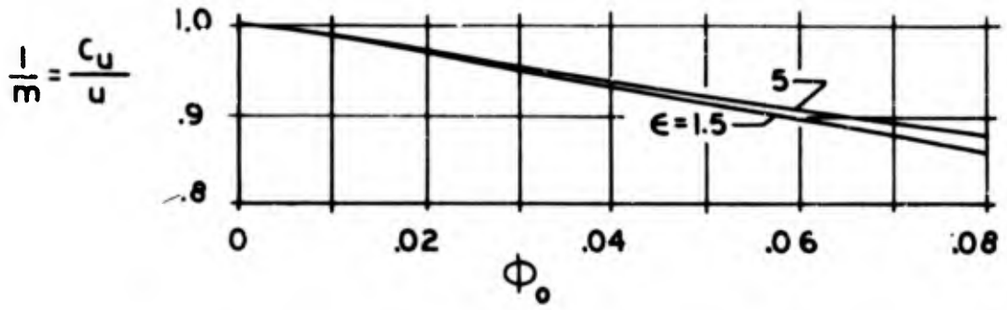

Figure 13. Slip Coefficient of Shear Force Rotor

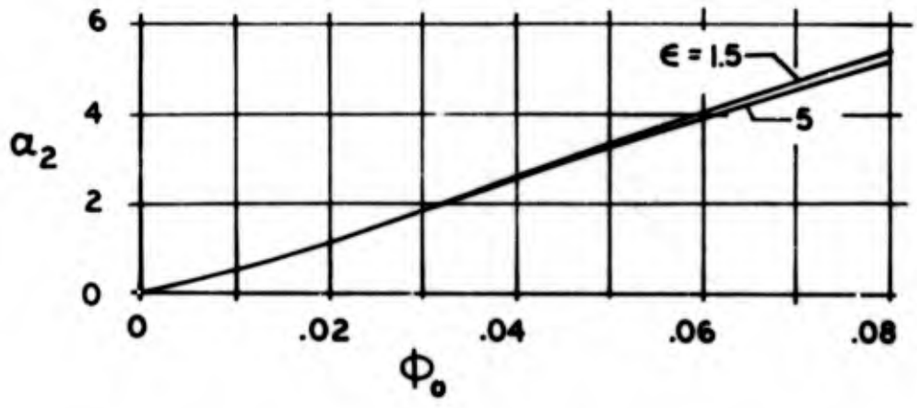

Figure 14. Flow Angle at Shear Force Rotor Discharge

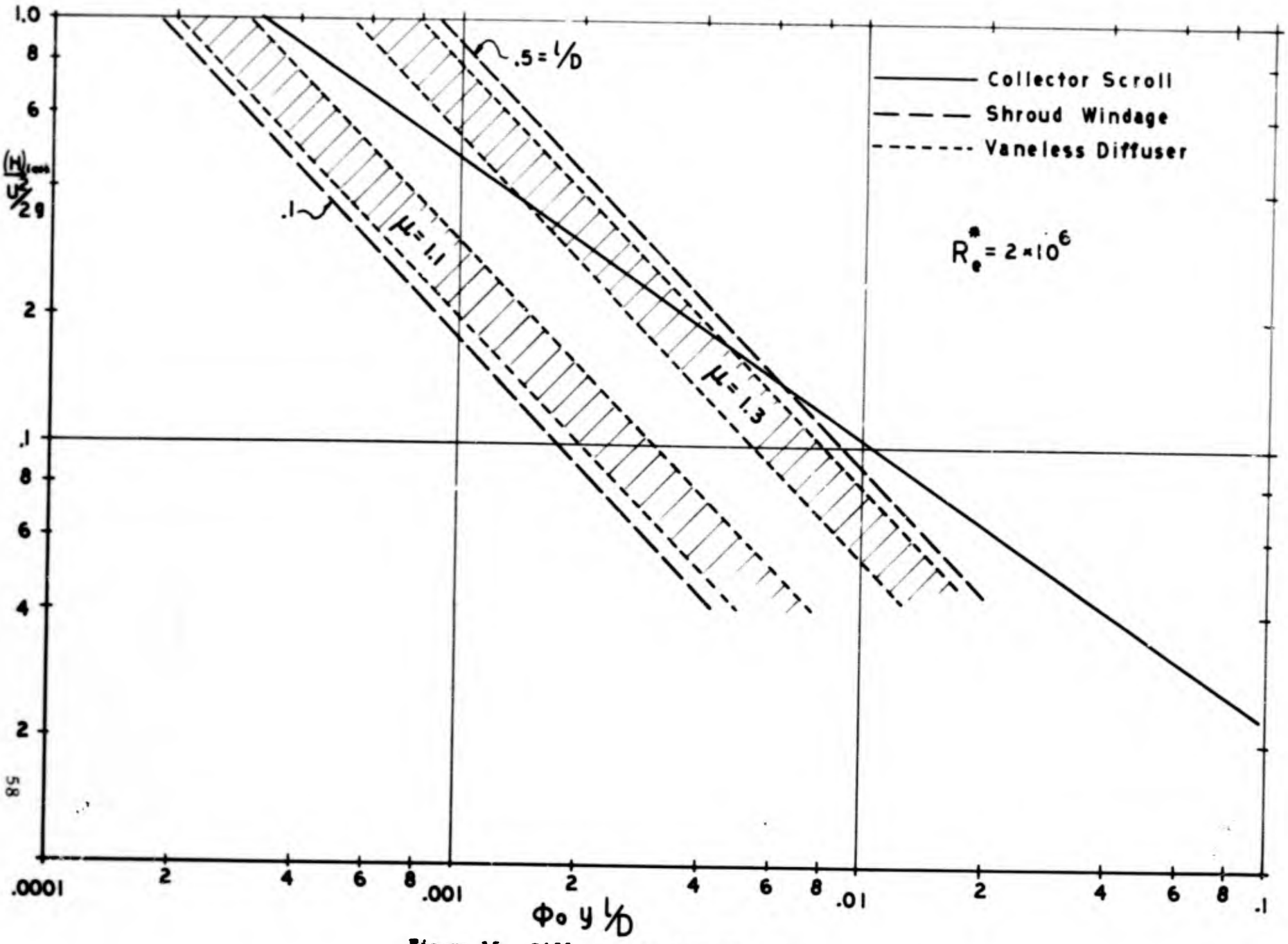

Figure 15. Diffuser Loss Presentation

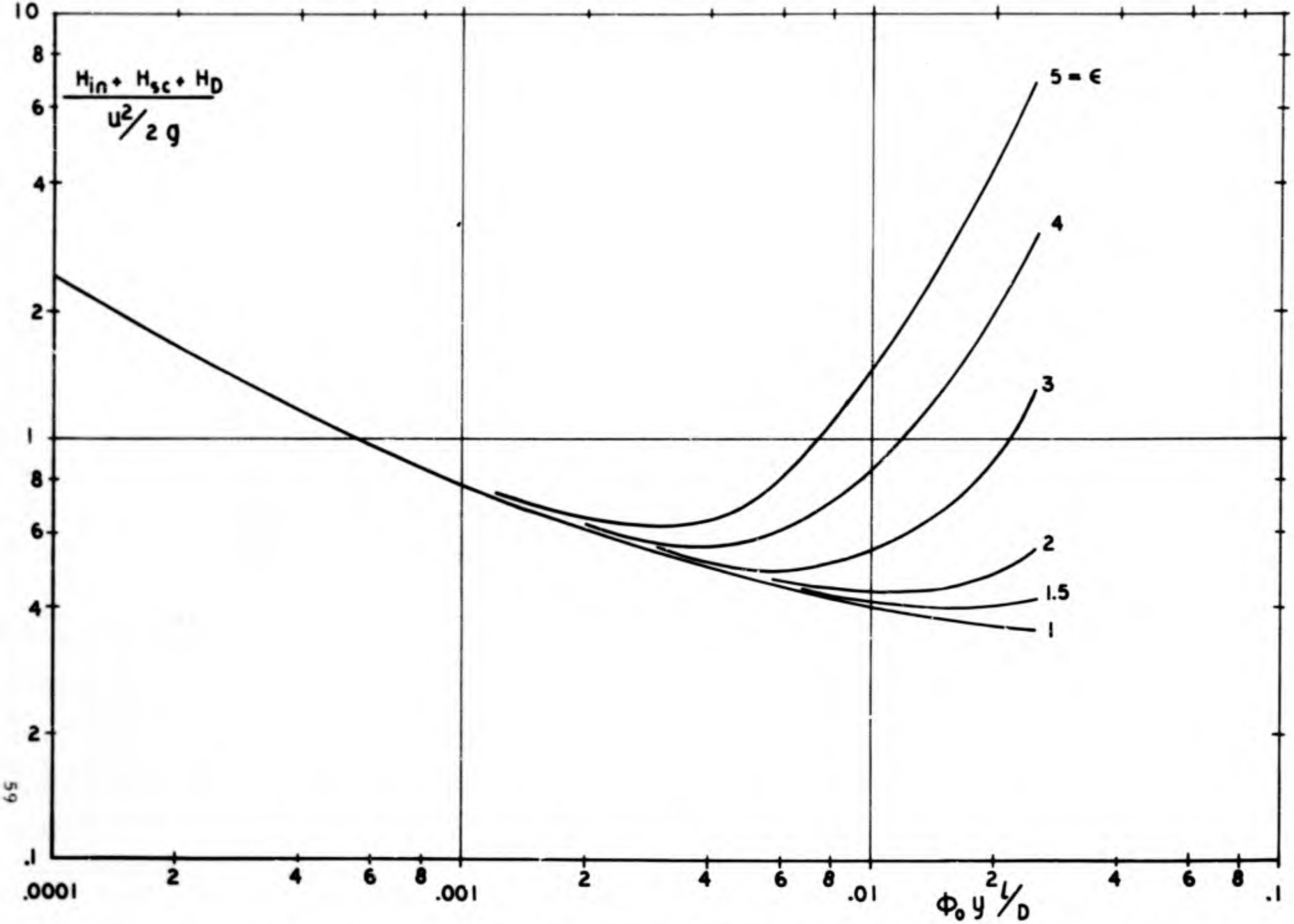

Figure 16. Rotor Inlet and Diffuser Loss for Shear Force Pumps

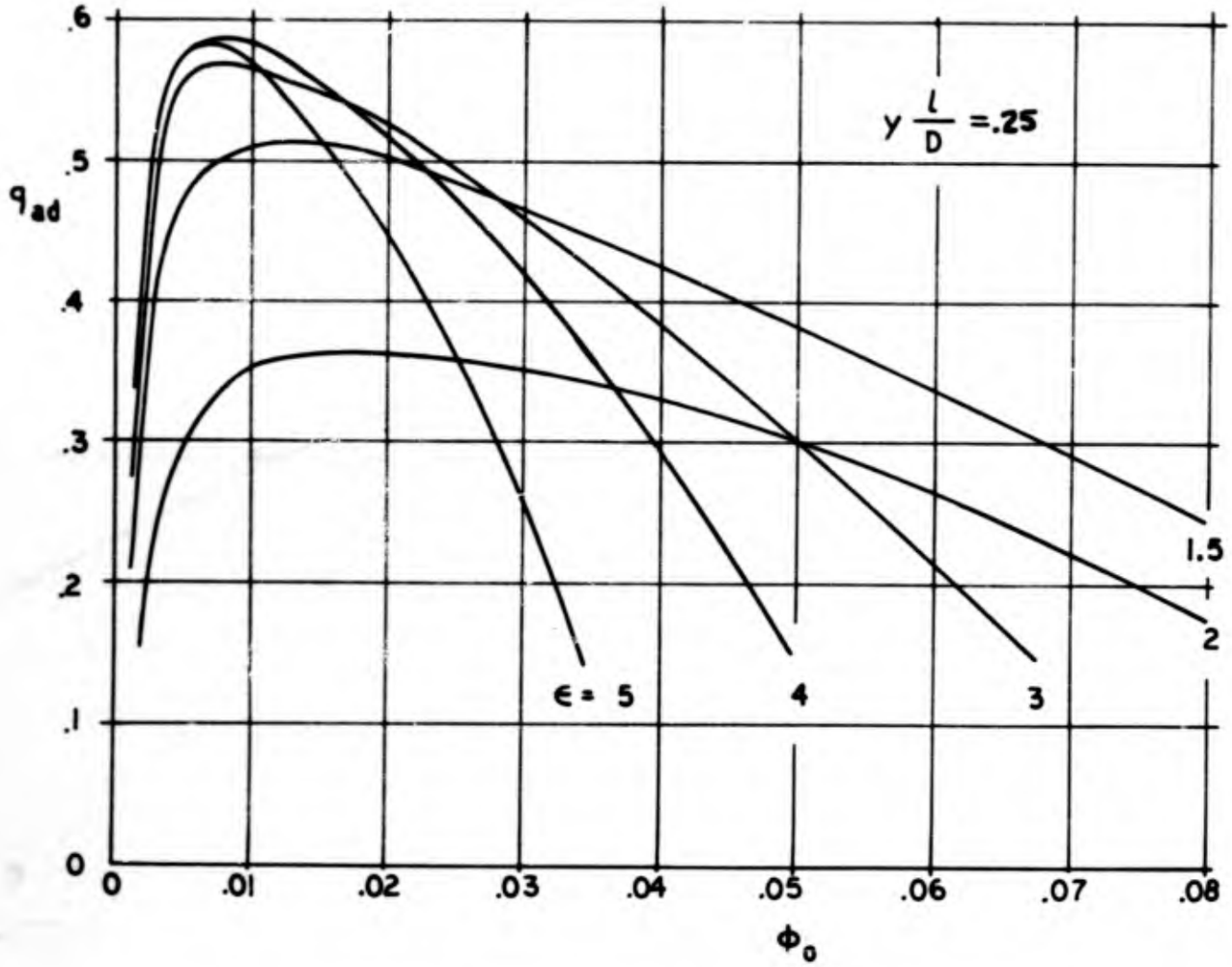

Figure 17. Calculated Head Coefficients of Shear Force Pumps

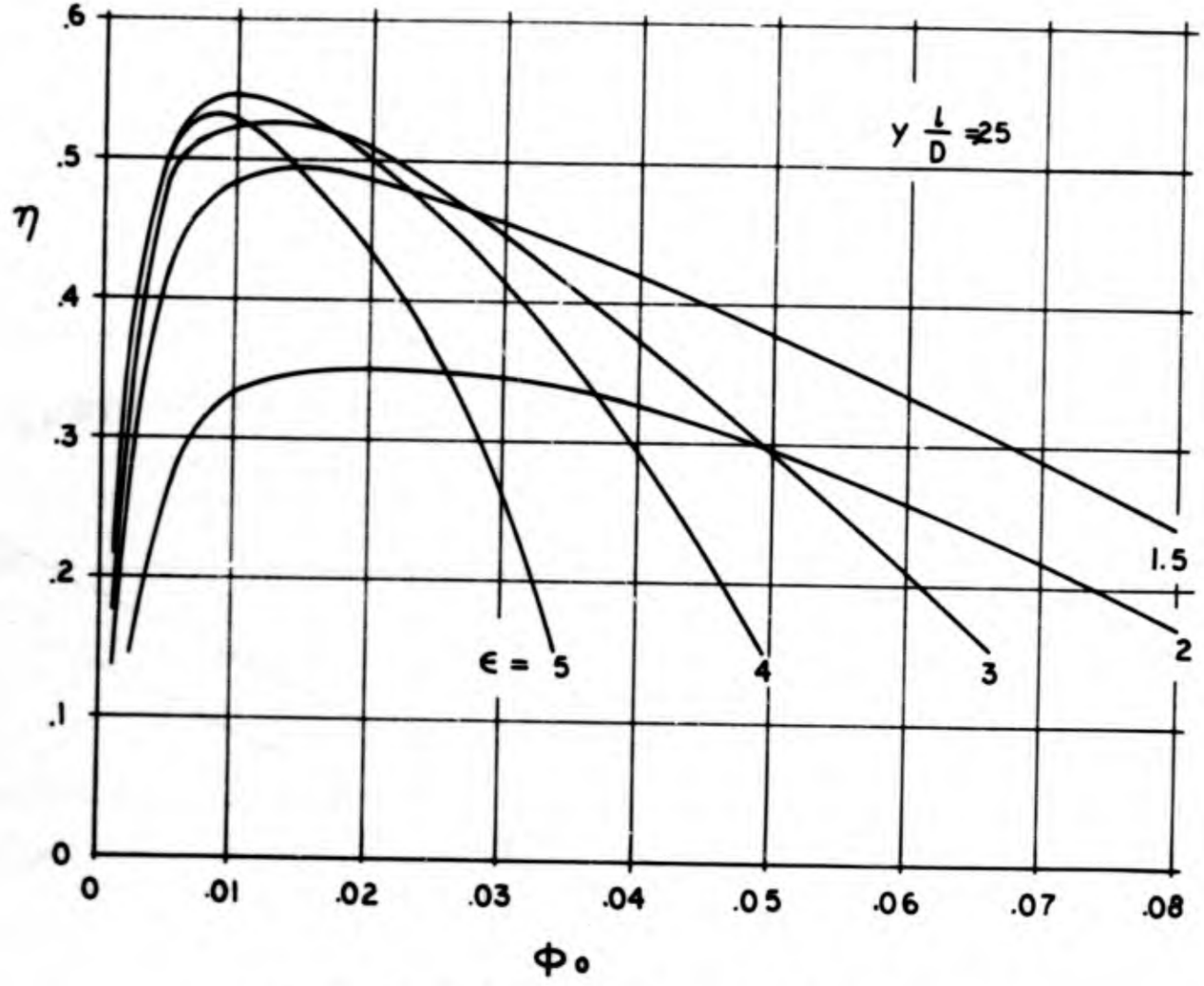

Figure 18. Calculated Efficiencies of Shear Force Pumps

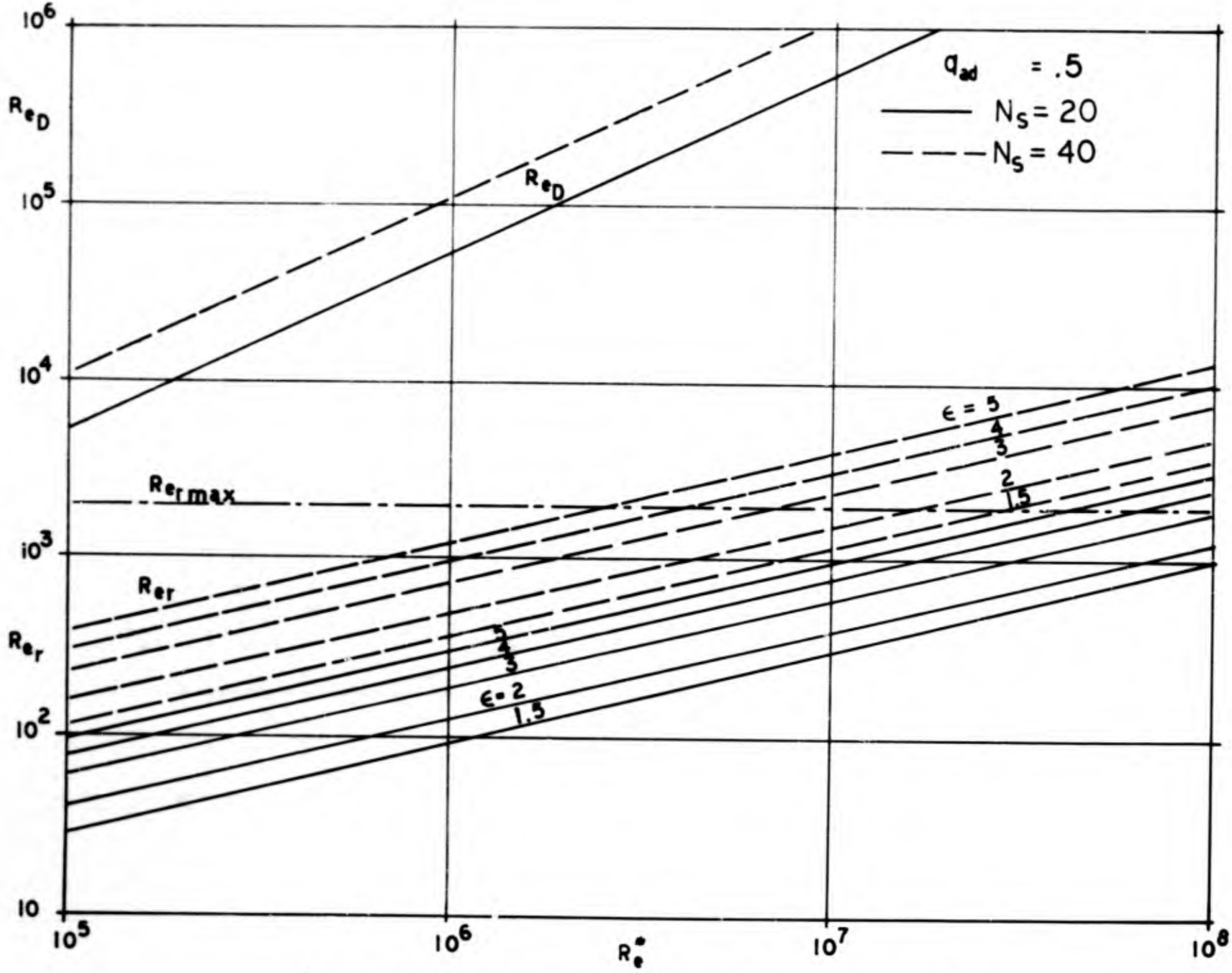

Figure 19. Reynolds Number Interrelations for Shear Force Pumps

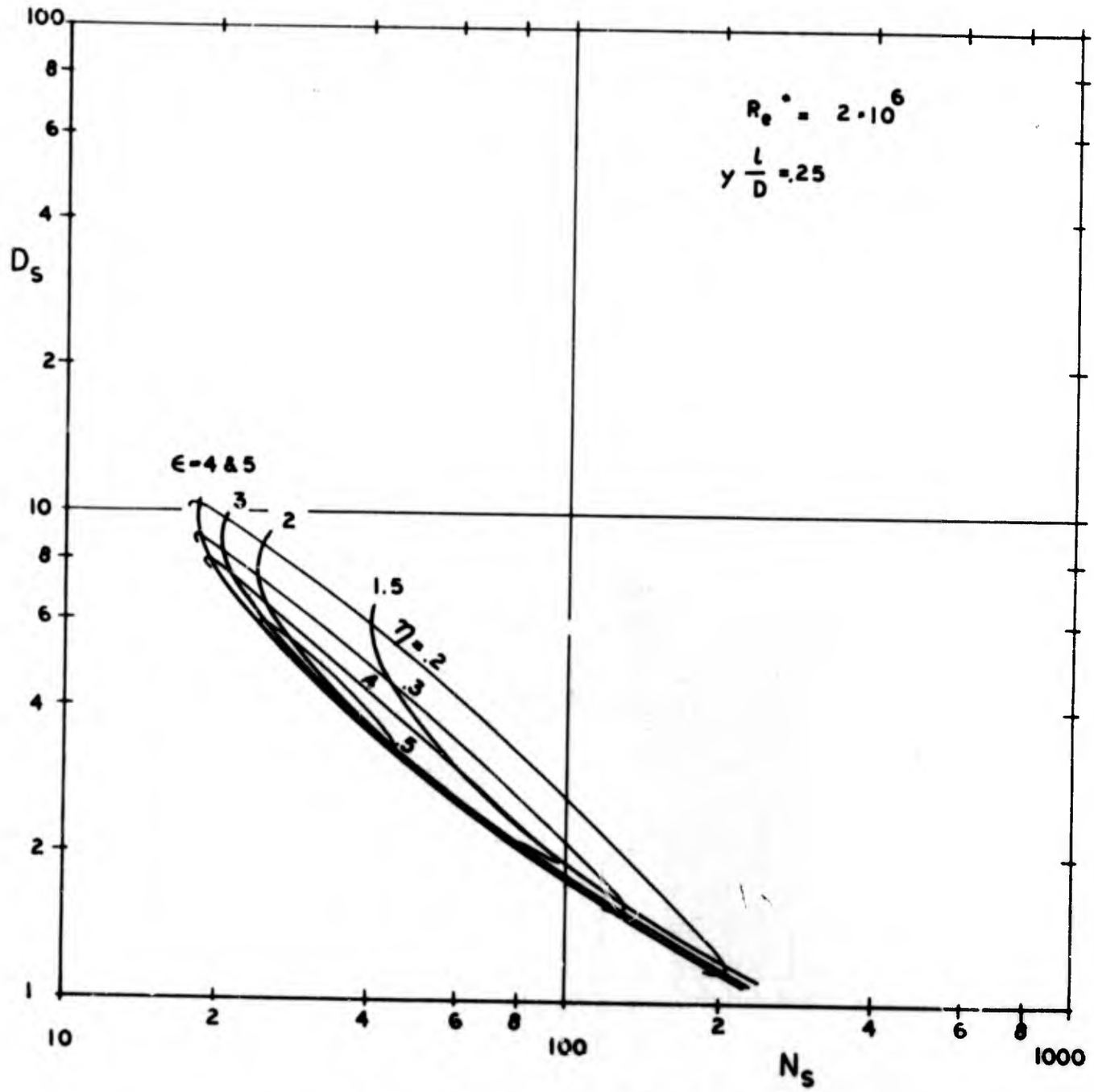

Figure 20. Calculated $N_s D_s$ Diagram for Shear Force Pumps

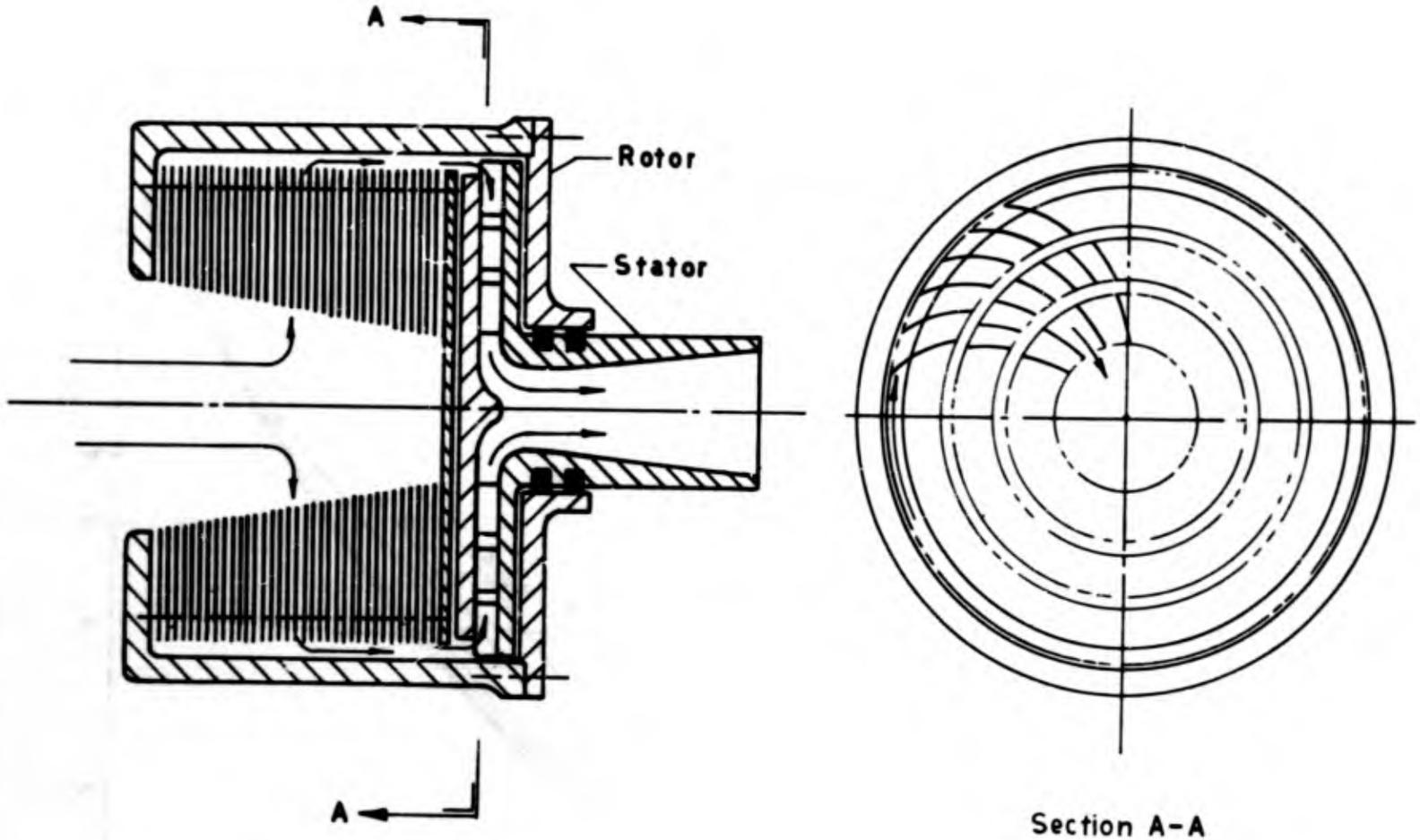

Figure 21. Shear Force Pump Configuration

Figure 22. Design Point Performance Comparison of She

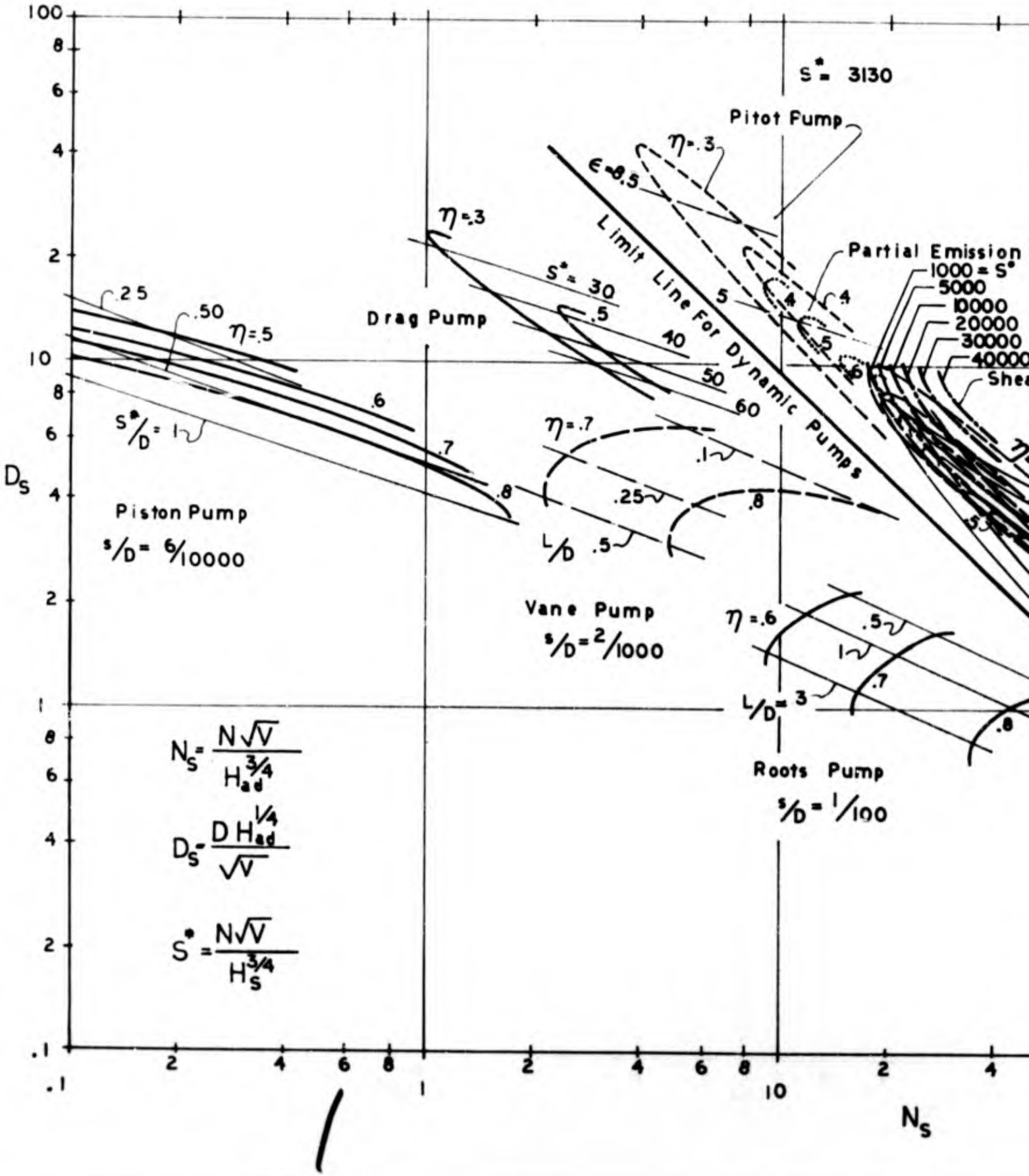

rmance Comparison of Shear Force Pumps and Conventional Pumps

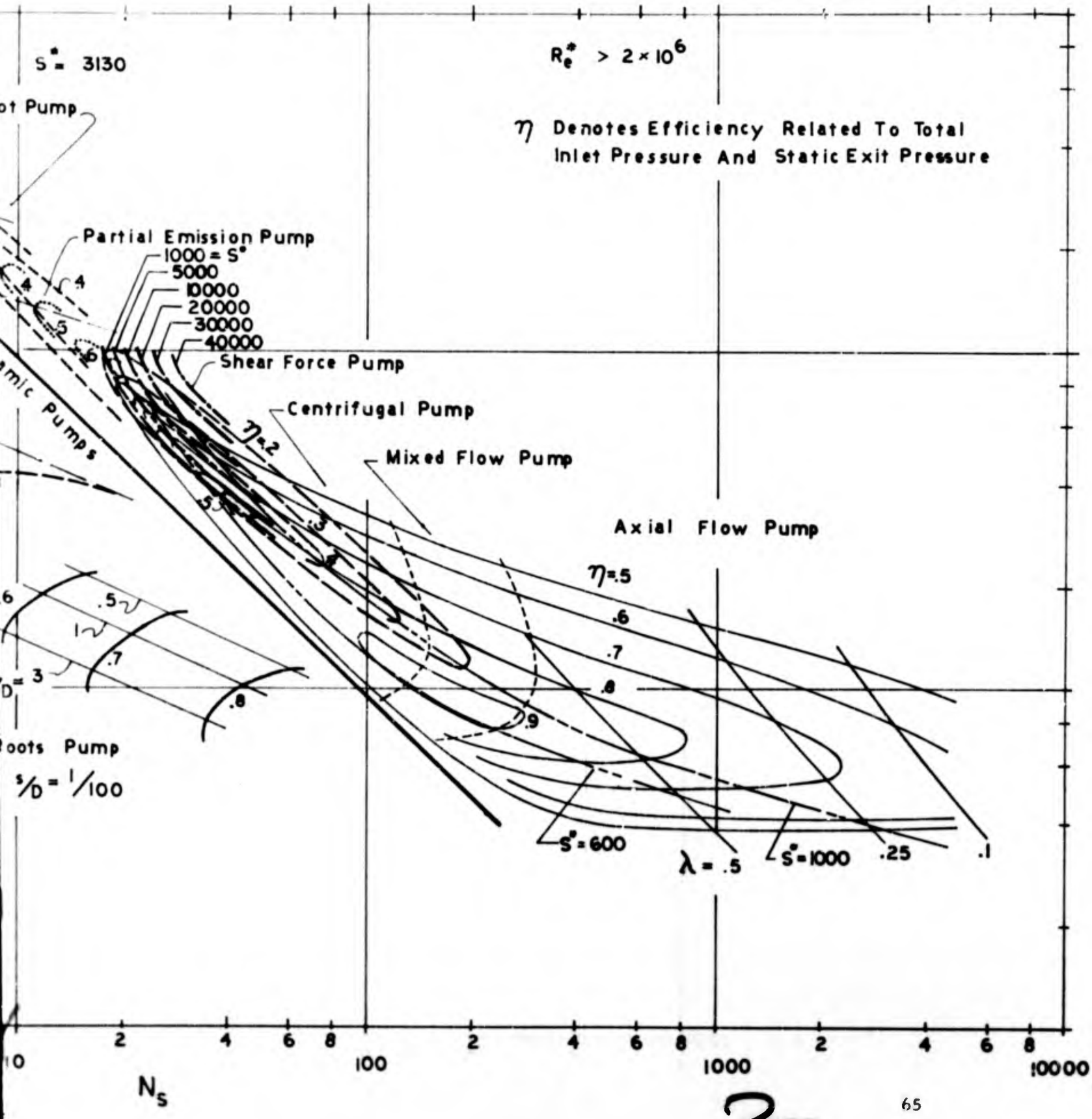

2

Figure 23. Suction Specific Speed Potential of Shea

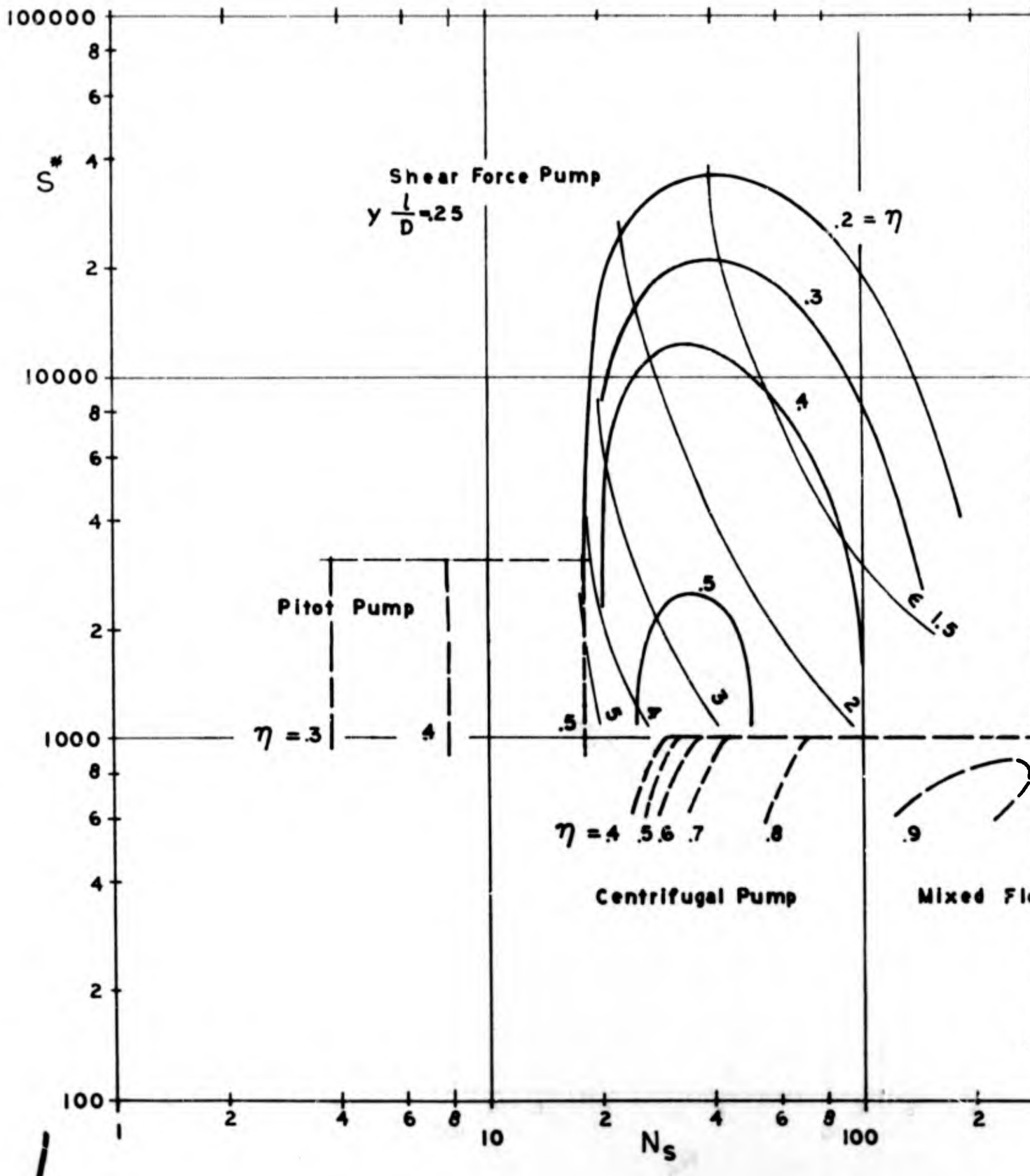

gure 23. Suction Specific Speed Potential of Shear Force Pumps

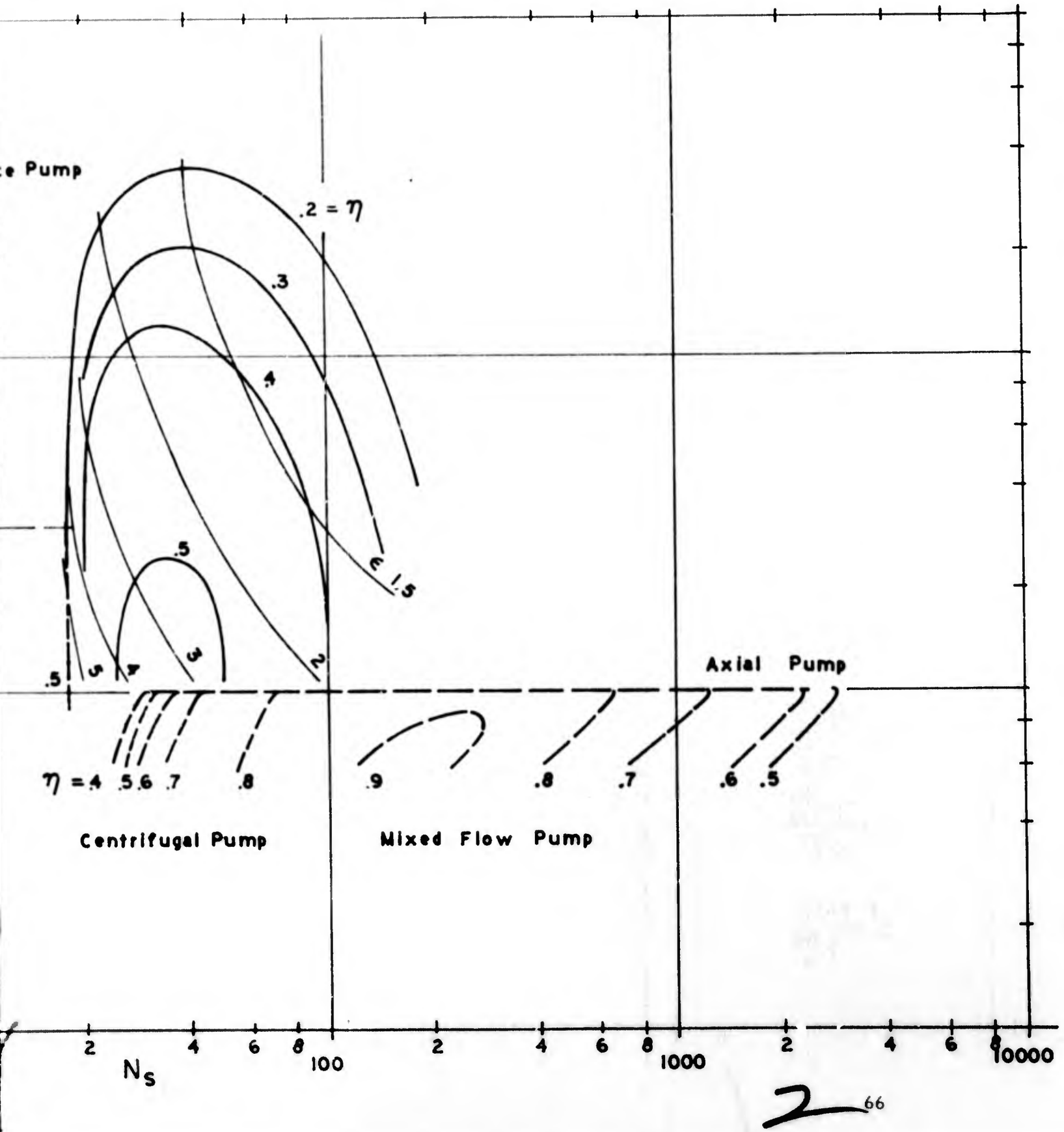

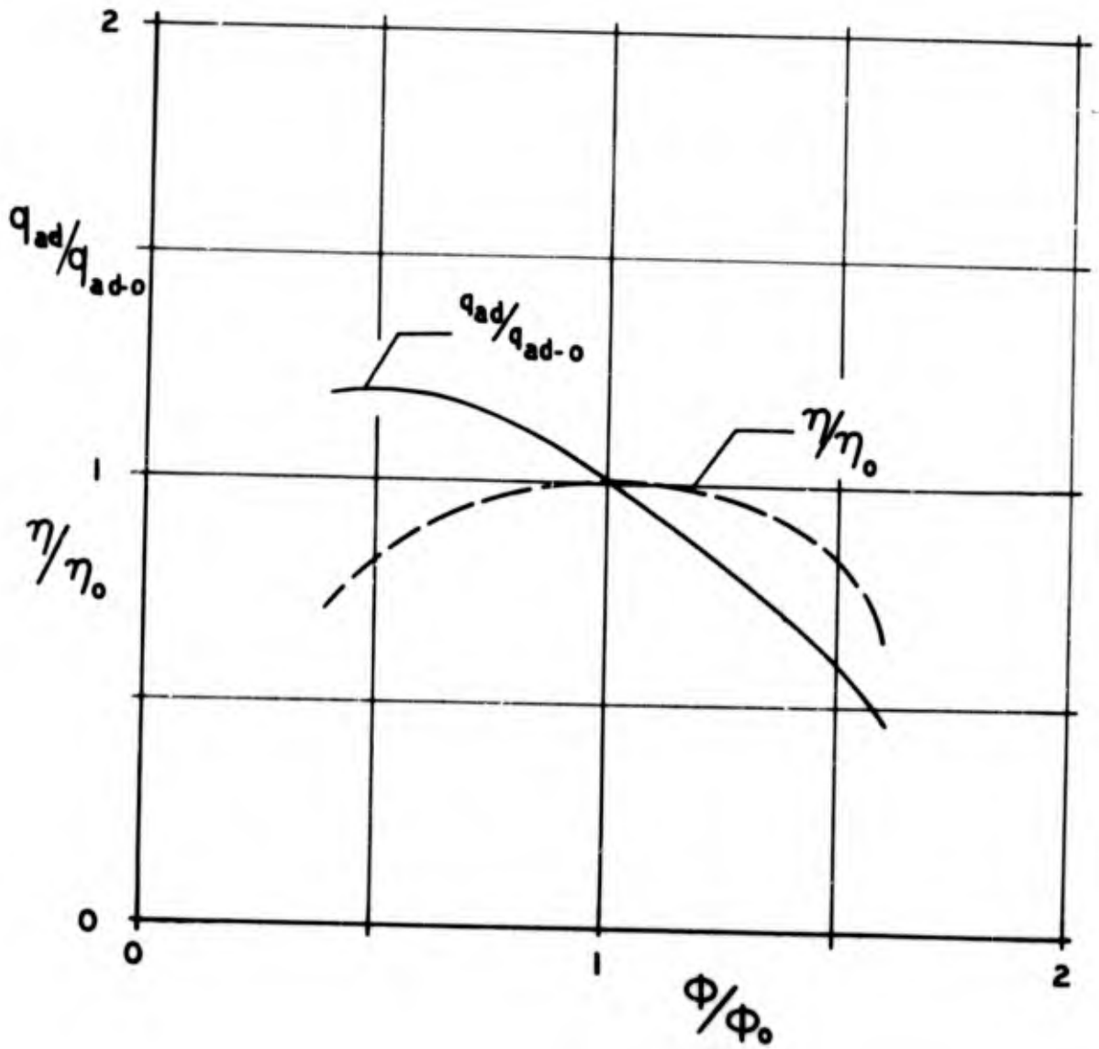

Figure 24. Typical Performance Characteristic of Conventional Pumps

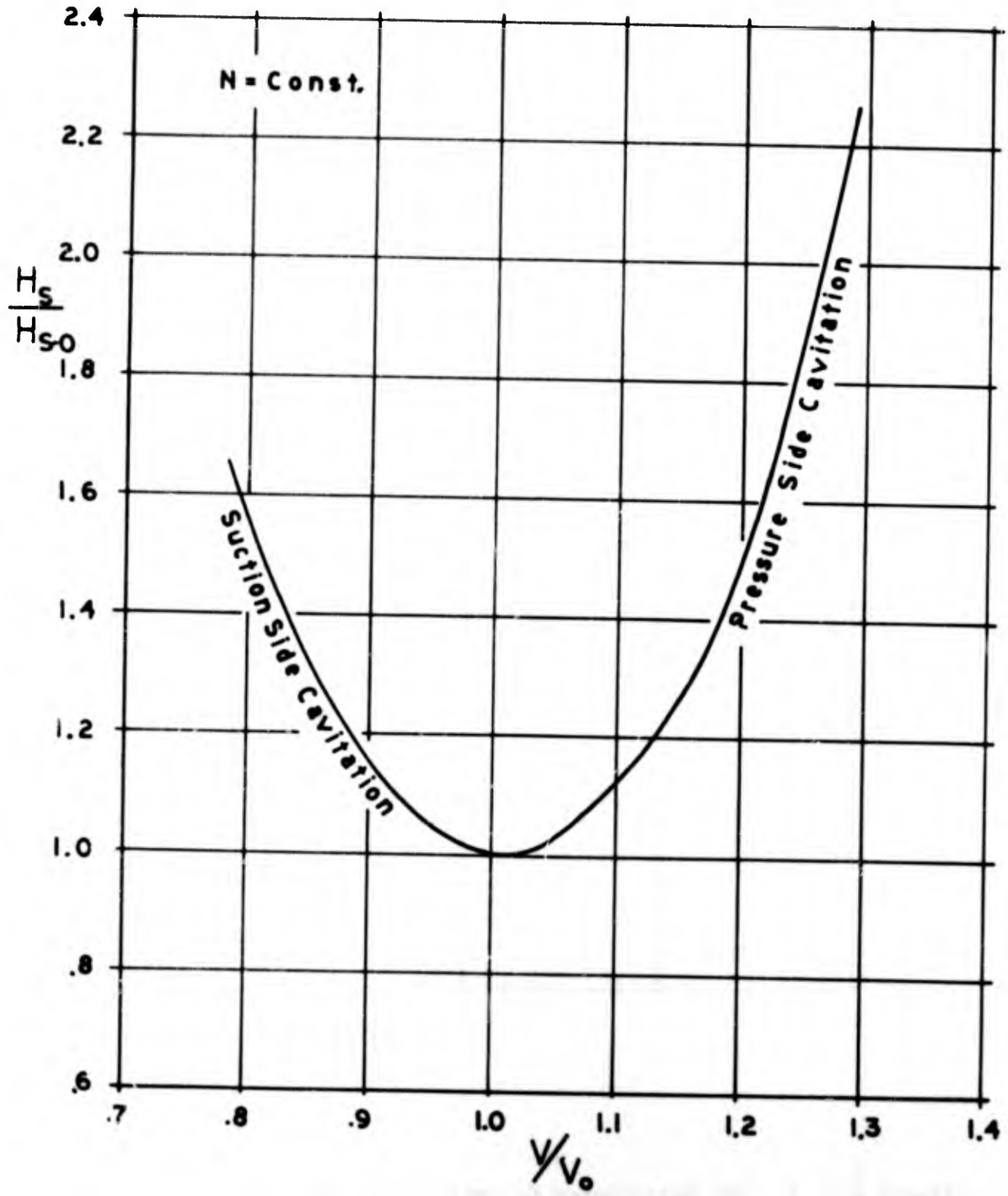

Figure 25. Typical Cavitation Behavior of Conventional Pumps

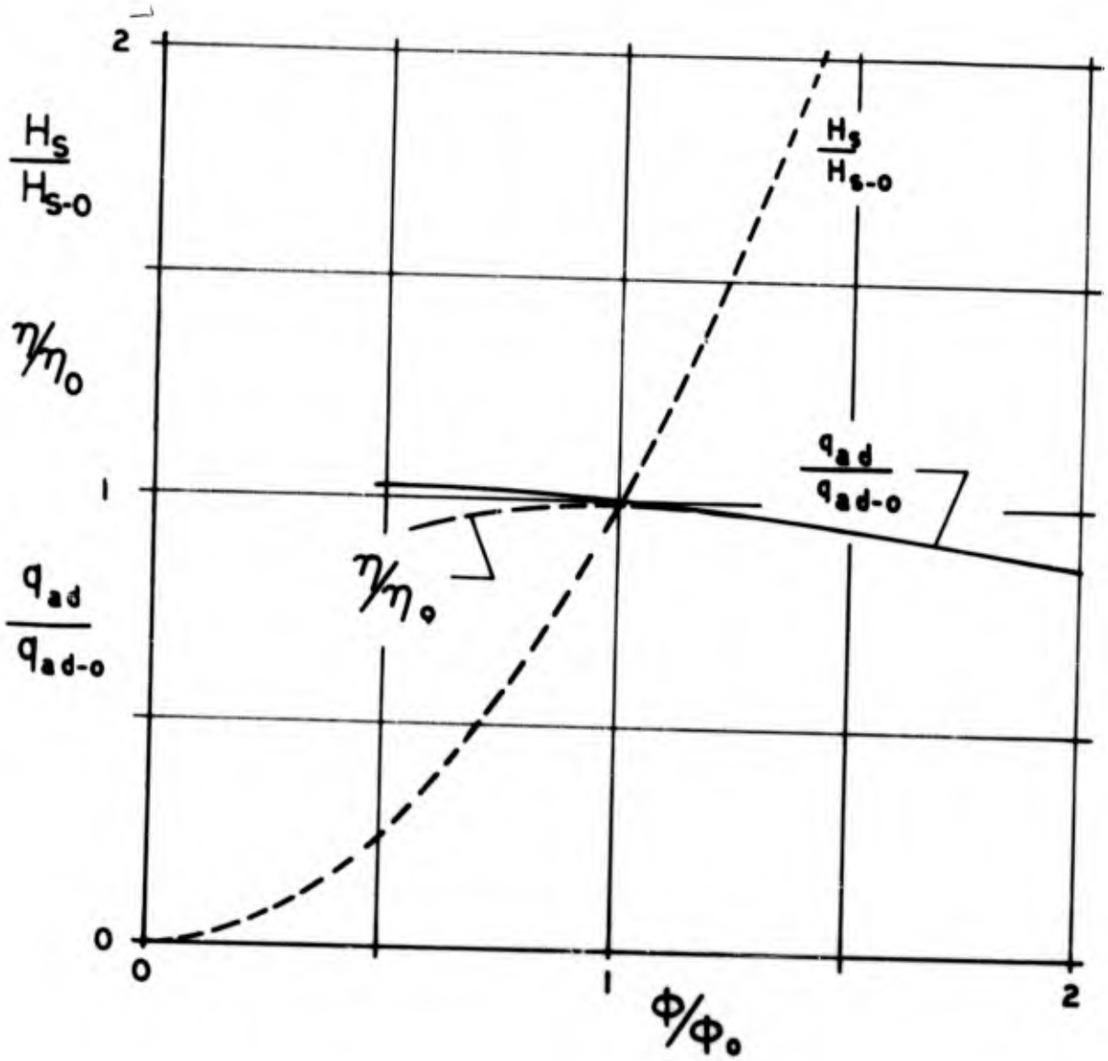

Figure 26. Typical Performance Characteristic of Shear Force Pumps

Unclassified

Security Classification

DOCUMENT CONTROL DATA - R&D

(Security classification of title, body of abstract and indexing annotation must be entered when the overall report is classified)

1 ORIGINATING ACTIVITY (Corporate author)

Dr. O. E. Balje, Engineering Consultant,
P.O. Box D, Sherman Oacks, Calif. 91413

2a REPORT SECURITY CLASSIFICATION

Unclassified

2b GROUP

3 REPORT TITLE

A Study of the Performance Potential of Conventional and Shear Force Pumps

4 DESCRIPTIVE NOTES (Type of report and inclusive dates)

Interim Report

5 AUTHOR(S) (Last name, first name, initial)

Balje, O. Erich

6 REPORT DATE

June 1965

7a TOTAL NO. OF PAGES

74

7b NO. OF REFS

15

8a CONTRACT OR GRANT NO.

AF 33(615)-1915

b PROJECT NO. 7116

c Task No. 7116-01

d

9a ORIGINATOR'S REPORT NUMBER(S)

9b OTHER REPORT NO(S) (Any other numbers that may be assigned this report)

ARL 65-118

10 AVAILABILITY/LIMITATION NOTICES

Qualified requesters may obtain copies of this report from DDC.

11 SUPPLEMENTARY NOTES

Release to OTS not authorized

12 SPONSORING MILITARY ACTIVITY

Aerospace Research Laboratory
Office of Aerospace Research, USAF
Wright-Patterson Air Force Base, Ohio

13 ABSTRACT

The design point performance of shear force pumps is compared with that of conventional pumps in terms of the similarity parameters specific speed, specific diameter and suction specific speed. Using arguments of the cascade theory, the maximum suction specific speed potential of conventional pumps is calculated for conventional as well as sophisticated blade design concepts. Comparing these data with experimental and theoretical data of shear force pumps, it was demonstrated that shear force pumps can obtain about 10 to 20 times higher suction specific speeds than conventional pumps in the medium specific speed regime, but that the efficiency potential of shear force pumps is lower than that of conventional pumps. The high suction specific speed potential of the shear force pump can be used advantageously in the design of compact lightweight space power plants.

DD FORM 1 JAN 64 1473

Unclassified

Security Classification

14 KEY WORDS	LINK A		LINK B		LINK C	
	ROLE	WT	ROLE	WT	ROLE	WT
Pumps Shear Force Pump Pump Parameters Cavitation						

INSTRUCTIONS

1. ORIGINATING ACTIVITY: Enter the name and address of the contractor, subcontractor, grantee, Department of Defense activity or other organization *(corporate author)* issuing the report.

2a. REPORT SECURITY CLASSIFICATION: Enter the overall security classification of the report. Indicate whether "Restricted Data" is included. Marking is to be in accordance with appropriate security regulations.

2b. GROUP: Automatic downgrading is specified in DoD Directive 5200.10 and Armed Forces Industrial Manual. Enter the group number. Also, when applicable, show that optional markings have been used for Group 3 and Group 4 as authorized.

3. REPORT TITLE: Enter the complete report title in all capital letters. Titles in all cases should be unclassified. If a meaningful title cannot be selected without classification, show title classification in all capitals in parenthesis immediately following the title.

4. DESCRIPTIVE NOTES: If appropriate, enter the type of report, e.g., interim, progress, summary, annual, or final. Give the inclusive dates when a specific reporting period is covered.

5. AUTHOR(S): Enter the name(s) of author(s) as shown on or in the report. Enter last name, first name, middle initial. If military, show rank and branch of service. The name of the principal author is an absolute minimum requirement.

6. REPORT DATE: Enter the date of the report as day, month, year, or month, year. If more than one date appears on the report, use date of publication.

7a. TOTAL NUMBER OF PAGES: The total page count should follow normal pagination procedures, i.e., enter the number of pages containing information.

7b. NUMBER OF REFERENCES: Enter the total number of references cited in the report.

8a. CONTRACT OR GRANT NUMBER: If appropriate, enter the applicable number of the contract or grant under which the report was written.

8b, &c, & 8d. PROJECT NUMBER: Enter the appropriate military department identification, such as project number, subproject number, system numbers, task number, etc.

9a. ORIGINATOR'S REPORT NUMBER(S): Enter the official report number by which the document will be identified and controlled by the originating activity. This number must be unique to this report.

9b. OTHER REPORT NUMBER(S): If the report has been assigned any other report numbers *(either by the originator or by the sponsor)*, also enter this number(s).

10. AVAILABILITY/LIMITATION NOTICES: Enter any limitations on further dissemination of the report, other than those imposed by security classification, using standard statements such as:

(1) "Qualified requesters may obtain copies of this report from DDC."

(2) "Foreign announcement and dissemination of this report by DDC is not authorized."

(3) "U. S. Government agencies may obtain copies of this report directly from DDC. Other qualified DDC users shall request through

_____."

(4) "U. S. military agencies may obtain copies of this report directly from DDC. Other qualified users shall request through

_____."

(5) "All distribution of this report is controlled. Qualified DDC users shall request through

_____."

If the report has been furnished to the Office of Technical Services, Department of Commerce, for sale to the public, indicate this fact and enter the price, if known.

11. SUPPLEMENTARY NOTES: Use for additional explanatory notes.

12. SPONSORING MILITARY ACTIVITY: Enter the name of the departmental project office or laboratory sponsoring *(paying for)* the research and development. Include address.

13. ABSTRACT: Enter an abstract giving a brief and factual summary of the document indicative of the report, even though it may also appear elsewhere in the body of the technical report. If additional space is required, a continuation sheet shall be attached.

It is highly desirable that the abstract of classified reports be unclassified. Each paragraph of the abstract shall end with an indication of the military security classification of the information in the paragraph, represented as *(TS), (S), (C), or (U)*

There is no limitation on the length of the abstract. However, the suggested length is from 150 to 225 words.

14. KEY WORDS: Key words are technically meaningful terms or short phrases that characterize a report and may be used as index entries for cataloging the report. Key words must be selected so that no security classification is required. Identifiers, such as equipment model designation, trade name, military project code name, geographic location, may be used as key words but will be followed by an indication of technical context. The assignment of links, rules, and weights is optional.